arXiv:0707.2252v1 [astro-ph] 16 Jul 2007

On the Rapid Collapse and Evolution of Molecular Clouds

Bruce G. Elmegreen

IBM Research Division, T.J. Watson Research Center, P.O. Box 218, Yorktown Heights, NY 10598, bge@watson.ibm.com

ABSTRACT

Stars generally form faster than the ambipolar diffusion time, suggesting that several processes short circuit the delay and promote a rapid collapse. These processes are considered here, including turbulence compression in the outer parts of giant molecular cloud (GMC) cores and GMC envelopes, GMC core formation in an initially supercritical state, and compression-induced triggering in dispersing GMC envelopes. The classical issues related to star formation timescales are addressed: high molecular fractions, low efficiencies, long consumption times for CO and HCN, rapid GMC core disruption and the lack of a stable core, long absolute but short relative timescales with accelerated star formation, and the slow motions of protostars. We consider stimuli to collapse from changes in the density dependence of the ionization fraction, the cosmic ray ionization rate, and various dust properties at densities above $\sim 10^5$ cm^{-3}. We favor the standard model of subcritical GMC envelops and suggest they would be long lived if not for disruption by rapid star formation in GMC cores. The lifecycle of GMCs is illustrated by a spiral arm section in the Hubble Heritage image of M51, showing GMC formation, star formation, GMC disruption with lingering triggered star formation, and envelope dispersal. There is no delay between spiral arm dustlanes and star formation; the classical notion results from heavy extinction in the dust lane and triggered star formation during cloud dispersal. Differences in the IMF for the different modes of star formation are considered.

Subject headings: stars: formation — ISM: magnetic fields — ISM: molecules

1. Introduction

Gas contraction during star formation can overcome magnetic forces in either of two ways, by diffusing through a supporting field or by overwhelming it with a greater force from self-gravity. If the equilibrium supporting field is termed critical, then the first of these is

subcritical contraction and the second is supercritical. In the standard model, clouds begin as subcritical throughout and spend a relatively long time (e.g., $\geq 10t_{dyn}$ for dynamical time t_{dyn}) contracting by ambipolar diffusion until their cores become supercritical, and then they spend a relatively short time ($1 - 2t_{dyn}$) collapsing to stars in the core (Mestel 1965; Nakano & Tademaru 1972; Mouschovias 1976; Shu 1983; Tomisaka, Ikeuchi, & Nakamura 1990; Li & Nakamura 2002). While there is a large body of literature on this subcritical to supercritical transition (see reviews in Shu, Adams, & Lizano 1987; Mouschovias 1991; McKee et al. 1993; Mouschovias, Tassis, & Kunz 2006), there is growing evidence that much of star formation actually begins closer to the supercritical state, bypassing the long diffusion time of the standard model (e.g., Nakano 1998; Hartmann et al. 2001).

This new view is based in part on the observation of infalling motions at large (~ 0.1 pc) radii (Tafalla et al. 1998; Williams et al. 1999; Williams & Myers 1999; Wu, Zhu, et al. 2005; Walsh, Bourke, & Myers 2006; Williams, Lee, & Myers 2006), which are expected for supercritical collapse (Basu & Ciolek 2004) and for supercritical collapse following fast inflows (Fatuzzo, Adams & Myers 2004). It is also based on the relatively short time scales for star formation (Lee & Myers 1999; Jijina, Myers & Adams 1999; Ballesteros-Paredes, Hartmann, & Vázquez-Semadeni 1999; Elmegreen 2000; Lee, Myers & Tafalla 2001; Myers 2005; Furuya, Kitamura & Shinnaga, 2006; Kirk, Ward-Thompson & André 2005, 2007; Jørgensen et al. 2007; see review in Ballesteros-Paredes & Hartmann 2007). Regarding these short time scales, it is important to distinguish between the duration of star formation once it begins in a cloud core, which is relatively short even in the standard model (Basu 1997; Tassis & Mouschovias 2004), and the total lifetime of the core, including the time prior to star formation. We consider here that even the total lifetime of giant molecular cloud (GMC) cores is relatively short, unlike in the standard model. The primary evidence for this is the short duration of star formation in cluster-forming cores (Sect. 3.2) combined with the low fraction of GMCs in a dormant, pre-star formation stage. There are no known examples of GMCs with potential cluster-forming cores hovering for $\sim 10t_{dyn}$ at subcritical masses while the magnetic field passively diffuses away. There are also few examples of the oblate shapes that are expected from slow-diffusion models (e.g. Ryden 1996).

Observations of magnetic field strengths show supercritical (i.e., weak) values directly (Troland et al. 1996; Roberts, Crutcher & Troland 1997; Bourke et al. 2001; Matthews et al. 2005) or values beyond (i.e., weaker than) supercritical (Crutcher 1999; Glenn, Walker, & Young, 1999; Uchida, Fiebig, & Güsten 2001; Brogan & Troland 2001). Indirect observations like bent or hour-glass field line shapes have been taken as evidence for supercritical fields too (e.g., Greaves, Holland & Murray 1995; Holland et al. 1996; Lai et al. 2002; Cortes & Crutcher 2006). Near-critical field values are also found in cloud cores (Bertoldi & McKee 1992; Curran et al. 2004; Cortes & Crutcher 2006), and subcritical values in cloud envelopes

(Cortes, Crutcher, & Watson 2005), but there are few or no subcritical values in GMC cores unless extreme orientations are assumed (Crutcher 2007).

Perhaps the biggest driver of our changing view is the recognition that supersonic turbulence is pervasive in the ISM. If a cloud is ever in quasi-equilibrium, then the presence of supersonic turbulence in addition to magnetic fields automatically implies rapid evolution toward supercritical cores and star formation. The turbulence always decays quickly, in $\sim t_{dyn}$ (Stone, Ostriker, & Gammie 1998; MacLow et al. 1998), and the magnetic field, having formerly shared the equilibrium support with turbulence, is suddenly alone and insufficient to prevent collapse. If star-forming clouds are never in equilibrium, then their evolution is rapid from the start. The same is true if molecular clouds are super-Alfvénic (Padoan et al. 1998, 1999), which means their turbulent speeds exceed their Alfvén speeds. The decay of this turbulence will rapidly convert these clouds to supercritical, leading to prompt collapse without a long diffusion stage. The remaining question is whether turbulence is regenerated during this collapse to sustain the cloud core life. We suggest in Sections 3.4 and 4 that it is not, at least where high mass stars form. Compressible turbulence inside a cloud core should not delay star formation but speed it up by increasing both the mass-to-flux ratio and the dynamical rate in the compressed regions (Sect. 3.5). The energy input also disrupts the core and moves the remaining parts of it and the envelope to the side where it forms more stars in another dynamical time (Sect. 4).

Evidently, the standard model of slow diffusion followed by rapid collapse has to be supplemented by two new modes of star formation in which gas becomes supercritical rapidly, in only one or two dynamical times following cloud formation. One of these new modes applies on a star-by-star basis, following turbulence-enhanced diffusion in compressed sheets and filaments in the cloud envelope (Elmegreen 1993; Fatuzzo & Adams 2002, Zweibel 2002; Heitsch et al. 2004; Fatuzzo, Adams, & Myers 2004; Li et al. 2004; Li & Nakamura 2004; Nakamura & Li 2005; Kudoh & Basu 2007). The other applies to a whole cloud core following a history of near-critical gas buildup and a brief diffusion phase (t_{dyn} to $2t_{dyn}$) that converts the core to supercritical (Ciolek & Basu 2001).

We propose here that massive cloud cores are born close to the critical condition. We make a distinction between rapid ($\sim t_{dyn}$) GMC core evolution and slow ($> t_{dyn}$) GMC envelope evolution. GMC envelopes are exposed to background radiation so they have high ionization fractions, and they apparently begin their lives in a subcritical state (e.g., Ciolek & Mouschovias 1995; Cortes, Crutcher & Watson 2005), while GMC cores are heavily shielded with low ionization fractions and they probably begin their lives in a critical state. In the absence of core star formation, GMC envelopes should last for several dynamical times, but because the envelopes form cores quickly, and the cores form highly disruptive stars quickly,

the envelopes are doomed along with their cores to have relatively short lives. This does not mean the envelopes are completely destroyed, however; their pieces are scattered and triggered to produce secondary generations of stars later. Some shredded pieces of GMC envelopes have the properties of diffuse clouds (e.g., Pan et al. 2005; Sect. 4).

The outline of this paper is as follows. Section 2 considers the rapid onset of supercritical conditions in GMC cores. Section 3 reviews the evidence for rapid star formation on large (3.1) and small (3.2) scales, the rapid evolution of HCN cores (3.3), the rapid dispersal of cluster-forming cores (3.4), the acceleration of magnetic diffusion in GMC envelopes (3.5), the possible enhancement of magnetic diffusion in GMC cores (3.6), and the slow motions of protostars (3.7). Section 4 illustrates the morphology of cloud formation, evolution, and destruction using the Hubble Heritage image of M51, and contrasts the points that GMC core evolution is supercritical and fast but GMC envelope evolution is subcritical and slow. Finally, the implications of rapid star formation for the IMF are reviewed in Section 5, where differences between supercritical cluster cores and turbulence-compressed GMC envelopes are suggested. A summary of the results is in Section 6.

2. Cloud Formation and the Onset of Critical Magnetic Support

Diffuse (i.e., non-self-gravitating) clouds form by localized compressions involving stellar pressures or supersonic turbulence generated on larger scales. They also form by shredding GMCs. The ISM is an active but relatively dark environment, so as long as the energy input is pervasive and fast while the temperature is low, shocks form easily and make diffuse clouds on dynamical time scales. Numerous simulations illustrate this process in detail (de Avillez & Breitschwerdt 2005; Piontek & Ostriker 2005). Diffuse clouds do not necessarily evolve into star-forming clouds. Some apparently do (Sect. 4), but most should disperse quickly in the turbulent flow pattern (Heitsch et al. 2006).

Self-gravitating clouds begin as diffuse clouds in the sense that their formation starts with a transition from non-self-gravitating to self-gravitating gas. This transition seems to be initiated most often on a galactic scale, where independent processes like spiral density waves, or directly related processes like swing-amplified gas instabilities and magneto-Jeans instabilities (Kim, Ostriker, & Stone 2002; Kim 2007) provide the environment for self-gravity to take hold. More localized compressions from stars (e.g., winds, supernovae, HII regions) and supersonic turbulence generated on larger scales also form self-gravitating clouds (e.g., Hartmann, et al. 2001), just as they form diffuse clouds. Because self-gravity is involved at some point in this formation process, whether at the beginning for the spiral instabilities or at the end for the collect-and-collapse scenarios, and because the induced motions which

start the latter are supersonic, the time scale for self-gravitating cloud formation is relatively short. That is, it operates in about a crossing time, which is also about the dynamical time, $t_{dyn} = (G\rho)^{-1/2}$.

For the topic of the present section, there are two important points: cloud formation itself does not involve or require magnetic diffusion, and self-gravitating cloud formation begins in an ambient ISM that is close to magnetically critical on a large scale. The first point illustrates again the relatively minor role of magnetic diffusion in star formation, limited, as it appears to be, to the final stages. The second point is directly related to the proposed rapid evolution of molecular cloud cores to supercritical collapse. The steps leading to this collapse are considered here.

The galactic dynamo pumps energy from shear and turbulence into the ambient magnetic field until the field pressure is comparable to the other energy densities that give the gas layer its thickness. Higher fields lose magnetic flux from the disk by the Parker (1966) instability. At the same time, galactic evolution with its cycle of self-gravitating cloud formation, star formation, and supernovae tends to pin the Toomre instability parameter Q at about unity (Goldreich & Lynden-Bell 1965). In that case, the self-gravitating energy density in the ISM is comparable to the other energy densities, and the disk thickness is about the ambient Jeans length. For these reasons, the magnetic energy density is comparable to the self-gravitating energy density on kpc scales in the main disks of spiral galaxies. Locally, both have a value of about 0.5 eV cm^{-3}. In this sense, the ambient ISM always has a near-critical magnetic field.

If we imagine a box with a height equal to the gas layer thickness (including HI) and a length and width equal to the inverse Jeans wavenumber parallel to the galactic plane, then the box is nearly cubical with all dimensions $\sim a^2/(\pi G\Sigma)$ for velocity dispersion a and mass column density Σ. This is the basic unit of self-gravitating cloud formation on a galactic scale: the basic unit for swing amplified and magneto-Jeans instabilities, and the basic unit for gas before a stellar spiral density wave shocks it into a filamentary dust lane. It might also be the outer scale for turbulence driven by gaseous self-gravity (Elmegreen, Elmegreen & Leitner 2003; Kim & Ostriker 2007). The mass of the basic unit for local conditions is 10^7 M$_\odot$ (much larger than a giant molecular cloud). The corresponding first step of self-gravitating cloud formation has been called either a supercloud (Elmegreen & Elmegreen 1983, 1987) or a giant molecular association (Rand & Kulkarni 1990) depending on the molecular fraction, which, in turn, depends on metallicity and pressure (Elmegreen 1993; Honma, Sofue & Arimoto 1995, Wong & Blitz 2002) and is unrelated to the cloud formation process.

We would like to know what happens to the state of magnetic criticality as this basic,

nearly-spherical, unit is distorted into various shapes by large-scale processes, and as the gas inside the unit recollects following these distortions into giant molecular clouds and their nearly-spherical cluster-forming cores. We show that every nearly-spherical, self-gravitating condensation that forms inside the basic unit will also be close to the critical field limit, regardless of intermediate steps, and that this preservation of criticality works quickly, on the dynamical time scale. In section 4 we discuss second-generation cloud core formation in the filamentary debris of first-generation GMCs; such filament streaming makes the cores more supercritical than the debris.

First consider the most fundamental definition of magnetic criticality, where the gradient in the field energy density, $\nabla B^2/4\pi$, equals the self-gravitating force density, $g\rho$, for field strength B, gravitational acceleration g and density ρ. Along a flux tube of halfwidth R, the first is $\sim B^2/4\pi R$ and the second is $2\pi G\rho^2 R$. Their equality gives the critical field strength $B = 8^{1/2}\pi G^{1/2}\rho R$. Similarly, for an infinite disk with a perpendicular mass column density Σ, the critical field is $B = 2\pi G^{1/2}\Sigma$ (Nakano & Nakamura 1978). The coefficients differ by only a factor of $2^{1/2}$. Here we write the critical field strength as $B = X\Sigma$ for constant X. For an equilibrium 3D configuration, the density and column density vary with position so either the central $B/\left(G^{1/2}\Sigma\right)$ ratio or the central mass M to magnetic flux flux Φ ratio are considered, or the total mass to magnetic flux ratio. Tomisaka, Ikeuchi & Nakamura (1988) find for the central value $G^{1/2}\Sigma/B = G^{1/2}M/\Phi = 0.17$, while Mouschovias & Spitzer (1976) find for the total cloud value $G^{1/2}M/\Phi = 0.13$. For generality, we write the critical mass to flux ratio as a constant $M/\Phi = Y$.

The mass to flux ratio is an indicator of stability only for spheroidal clouds, which are bounded in 3 dimensions. Suppose a large round cloud threaded with field lines is critical with both $B = X\Sigma$ and $M/\Phi = Y$; these expressions have the same meaning for a round cloud. A thin tube of flux inside this cloud has about the same B and ρ but a smaller radius $r << R$, and so it is magnetically sub-critical ($B >> X\rho r$) by the first definition. However the flux in this tube is smaller than the flux in the whole cloud by the ratio $(r/R)^2$, and the mass in the tube is smaller than the whole cloud by the same ratio, so the mass to flux ratio of the tube is the same as in the whole cloud: $M/\Phi = Y$. Turbulence compression perpendicular to the magnetic field can form a small tube of flux like this. To be specific, suppose compression changes the cross-field dimension in part of the cloud by the geometric-mean factor C (i.e., $C = R/r > 1$). Then without magnetic diffusion, both the flux and the mass in this compressed region are the same as they were before, rendering M/Φ unchanged at the value Y. At the same time, B increases by C^2 and Σ by C, so B/Σ goes up by the factor C to the value XC. Such a compressed region is stable in the transverse direction because it would expand back without the confining ram pressure of the turbulent flow around it. Thus the B/Σ condition, which indicates stability in this example ($XC > X$), is

more fundamental for diverse geometries than the M/Φ condition.

Now consider what happens to the state of criticality as gas flows along the field lines in the compressed filament, collecting into N cores of height H spaced out along its total length L. The mass in each is the initial mass of the filament divided by N, so M/Φ decreases from Y to the sub-critical value Y/N. The transverse column density in each increases during this collection by the factor L/NH, so B/Σ becomes $XCNH/L$. If both the cores and the original cloud are somewhat spherical, then $C \sim L/H$ and the first condition also becomes subcritical, by the same factor N: $B/\Sigma \sim XN$. Thus the cores are stable by the same degree for both conditions. For them to form stars, magnetic diffusion has to reduce the flux by a factor N. *The observation of protostars or dense mm-wave continuum sources strung out along filaments implies that significant magnetic diffusion has already occurred.* During this diffusion, both criticality conditions move together from sub-critical to super-critical. (We note that turbulence simulations without magnetic fields also get beaded filaments, but this field-free case is unrealistic. The same result in the magnetically critical case requires diffusion.)

Compression parallel to the field should also be considered. Suppose part of the cloud of length $L < R$ is compressed along the field into a layer of thickness H, so the density and transverse column density (perpendicular to the field) go up by the factor L/H. The field strength will be unchanged at first by the parallel motions so B/Σ decreases to the *super*-critical value XH/L. The M/Φ ratio drops for the layer because, although the flux is constant, only part of the total cloud mass is involved; this gives $M/\Phi \sim YL/R$, a *sub*-critical value. However, the layer will be heavily weighed down transverse to the field and it will adjust, pulling in the field with it. Because B increases as the inverse of the transverse area and Σ increases only as the inverse of the transverse length, the ratio B/Σ goes back up and eventually becomes X, stabilizing the collapse. This stable point occurs when the new transverse radius is $r \sim RH/L$. The transverse collapse preserves both mass and flux in the layer, so M/Φ stays with its sub-critical value YL/R. Thus the new core is critical by the first condition and sub-critical by the second condition. However, prior to the initial compression, this part of the cloud had the same low M/Φ ratio as it did after the compression and collapse: the mass was down by the factor L/R at both times. Thus both B/Σ and M/Φ are unchanged after the adjustment for this part of the cloud. Moreover the final condensed object will be spheroidal if the transverse size, $r \sim RH/L$ equals the parallel height, H, and this requires $L \sim R$. Thus parallel compressions and equilibrium adjustments in spherical clouds leading to spherical cores will leave the state of criticality unchanged if there is no magnetic diffusion.

In general, there will be compressions from turbulence and external pressures both trans-

verse and parallel to the field, and at oblique angles, and the compressed gas will re-adjust by self-gravitational forces forming dense cores. Transverse components of compression tend to make cores with a decreased state of criticality (for $N > 1$ in the above example) and these cores will survive only during the active compression unless there is significant flux loss at this time. Parallel components of compression tend to preserve the state of criticality even without flux loss. If the characteristic length for collapse along a transversely-compressed filament is much longer than its width (as suggested by theory – Fiege & Pudritz 2000), and comparable to its length, then only $N = 1$ core will form in the transverse-compressed filament and both directions of compression produce cores with the same state of criticality as the initial cloud. In this case, cloud formation by self-gravitational readjustment of compressed and distorted basic ISM units will produce whole GMCs at about the same state of magnetic criticality as the ambient medium. Similarly, the round cores of GMCs, however they form, will begin their lives close to the state of magnetic criticality of the surrounding cloud. As the ambient ISM is approximately magnetically critical, so the clouds and cluster-forming cores will be too, before any diffusion begins. Vázquez-Semadeni et al. (2005) also noted that spheroidal supercritical cores require spheroidal supercritical clouds in the absence of magnetic diffusion.

We note that conservation of magnetic criticality from a large spheroidal cloud to a small spheroidal cloud implies significant movement of gas along the field lines in the absence of magnetic diffusion. We are suggesting this is the case. Such parallel motion does not happen all at once, however, but in steps as the GMC and GMC core form in a hierarchical fashion from self-gravity and turbulence compression. The parallel motion is also accompanied by perpendicular motion to preserve cloud roundedness, but the latter moves the field with it, causing the observed hour-glass shape with a pinch at the middle. Eventually magnetic diffusion smooths out the field, but this smoothing is not needed for GMC core-formation, which operates quickly. A typical GMC is 1% the mass of a supercloud (10^5 $M_\odot$ compared to 10^7 $M_\odot$), and 10% of the size ($100 \times 20 \times 20$ pc^3 compared to $1000 \times 200 \times 200$ pc^3). This means the GMC is a contraction of the inner $100^{-1/3} \sim 0.2$ of the supercloud length by a factor of only ~ 2. Similarly, a cluster-forming core might be $\sim 10\%$ of the GMC mass and 20% of the size, which means that $10^{-1/3} = 0.46$ of the GMC length is involved in core formation with a contraction that is another factor of ~ 2. Most of the supercloud mass stays in a low density envelope that has little star formation, and most of the GMC mass stays in another, denser envelope where star formation is also relatively slow. The two factors of 2 illustrate the modest amount of motion along field lines and the mild perpendicular re-adjustment to this motion. The smallness of these factors helps explain the quickness of GMC and GMC core formations.

At this point in the evolution of a cloud, it takes only a little magnetic diffusion for the

core to become supercritical and begin a collapse phase. Whereas the usual diffusion time is $t_B = R/\Delta v$ for ion-neutral drift velocity Δv and cloud radius R, the diffusion time to reach a supercritical state from an initial state with $B = aX\Sigma$ and a slightly larger than 1 is only $t_B\,(1 - 1/a) << t_B$. This is because Σ has to increase by $1/a$ to become supercritical, and for transverse motions $\Sigma \propto 1/R$. Thus the core gas has to diffuse only from an initial radius R to a slightly smaller radius R/a for the core to go supercritical, and the time scale for this is $(R - R/a)\,/\Delta v = t_B\,(1 - 1/a)$. A more detailed discussion is in Ciolek & Basu (2001). They get $t_{core} \sim t_B\,(1 - M/Y\Phi)$ for marginally subcritical cores, and this is about the same result.

3. Time Scale for Star Formation

3.1. The Big Scale

One of the most revealing diagnostics of the star formation process is the time scale. If it is long compared to the dynamical time, then mechanisms for delay and prevention of star formation in strongly self-gravitating gas have to dominate the process. If the ratio of times is of order unity, then the gas collects into stars as fast as physically possible.

Modern observation suggest that star formation is much faster than we imagined three decades ago, when a time scale of $\sim 10^8 - 10^9$ yrs came from the ratio of Galactic molecular mass to star formation rate (Zuckerman & Evans 1974; Scoville & Solomon 1975) and from the high molecular fraction of the inner Milky Way (Solomon, Sanders & Scoville 1979). The GMC evolution times dropped to 30 Myr when the interarm regions were found to be mostly free of GMCs (Bash, Green & Peters 1977), and to 5-10 My when the ages of newly exposed clusters were first observed (Leisawitz, Bash & Thaddeus 1989). Now the formation times of dense clusters can be observed directly, suggesting that the main star formation activity is often over in ~ 3 Myr. Inside the denser cores where individual stars form, it can be as short as several $\times 10^5$ years (e.g., Onishi et al. 2002). In the LMC, GMC lifetimes may be a little longer $\sim 10 - 30$ Myr for reasons that are unexplained (Fukui 2007; Kawamura et al. 2007).

All of these time scales are still correct in the sense that the basic observations have not changed. The interpretation of what they mean has changed, however. The high molecular fraction in the inner Milky Way implies that gas spends a high fraction of its time in molecular form without forming stars. This means some combination of four things: (1) star formation is inefficient in CO clouds; (2) molecular envelopes contain most of the CO mass but evolve more slowly than the dense molecular cores where stars form; (3) molecular clouds get

dispersed in CO-rich pieces after star formation, and (4) some molecules are in diffuse clouds that do not form stars (Polk et al. 1988).

These four points are familiar: self-gravitating clouds are assembled by gravitational collapse in spiral density wave shocks, turbulent shocks, and explosive shells, and they form by gravitational instabilities in the ambient medium as part of swing-amplified spiral growth. These are all dynamical processes that operate as quickly as possible in the ISM, such as the crossing time over the scale height, $H = a^2/\pi G\Sigma$, or the self-gravity rates $(G\rho)^{1/2}$ and $\pi G\Sigma/a$ for average midplane density ρ, disk column density Σ and velocity dispersion a. The clouds then evolve to high density on the internal dynamical time scale which decreases as the density increases. Molecules form in clumps as soon as the cloud can shield itself, which is at a relatively low average density for a massive cloud (e.g., Pelupessy, Papadopoulos, & van der Werf 2006; Glover & Mac Low 2007), and stars form slightly later. The main point here is that even though every step operates at close to the local dynamical rate, the star formation step operates at the highest density where the dynamical rate is greatest. Cloud core disruption is also at the high core rate, via shocks from winds and HII regions. Thus self-gravitating clouds spend a longer time forming than getting dispersed even though every step evolves as quickly as possible: the relevant density is lower when they form than when they get dispersed.

Cloud destruction after star formation involves mostly the dense core. Part of the GMC envelope will get compressed during core disruption and form new stars as a result, and part will get pushed away with only scattered star formation before settling into new cores. In either case, a large fraction of the GMC molecules outlasts the first generation of star formation in the core, which typically involves only $\sim 10\%$ of the GMC mass. If the ratio of the core density to the average density in a GMC is ~ 100, then the ratio of dynamical times is ~ 10, and the envelope molecules last ~ 10 times longer than the star formation event. The fraction of GMCs that are active is not 10%, however. The timing factor of 10 has to be divided by the number of dense-core locations and generations per GMC. Considering that the Orion cloud formed ~ 4 generations and other local clouds form a similar number of subgroups, and that star formation usually persists at a relatively low level on the periphery of OB associations even after the dense core phase is over, the inactive GMC fraction is very low. Thus the fraction of the ISM in the form of GMCs can be high, as it is in the inner Milky Way, even though each stage prior to star formation evolves at the local dynamical rate. The star formation rate is low, only $\sim 1\%$ of the dynamical rate for the average GMC, because $\sim 90\%$ of the GMC mass has a long dynamical time, and $\sim 80 - 90\%$ of a GMC core gas gets dispersed during star formation (i.e., cluster formation in dense cores is only $\sim 10 - 20\%$ efficient; e.g., Tachihara et al. 2002; Lada & Lada 2003; Brooke et al. 2007; Jørgensen et al. 2007).

It is important to make a distinction here between GMC destruction, where the GMC is converted back into atomic form, and GMC dispersal, where the GMC is moved and broken apart. Both lead to the end of star formation in any one location, but the relevant time scales and processes differ and their contributions to the total molecular fraction differ. GMC destruction requires ionization and heating, so the cloud is disassembled molecule by molecule. Ionization can destroy part of a GMC, but ionization is usually accompanied by compression and motion, so the cloud moves away in pieces before it is completely destroyed. Whitworth (1979) estimated that the ionized mass from an embedded OB cluster is $2.3 \times 10^4 \, (T_i/5 \text{ Myr})^3 \, (\epsilon/0.04)^{4/3} \, (n/10^3 \text{ cm}^{-3})^{-1/3} \; M_\odot$ for ionization time T_i, star formation efficiency ϵ and cloud density n. With shorter O-star lifetimes than he assumed, $T_i \sim 3$ Myr, and slightly lower ϵ for whole OB associations (e.g., 1% per generation for average GMCs according to Williams & McKee 1997), the ionized mass is only $10 - 20\%$ of a GMC mass. Thus there is usually a large mass from the GMC envelope left over after cluster formation in the core, and this mass is available for more star formation in a slightly different location after another dynamical time (Sect. 4).

It is also important to distinguish between timescales for GMC destruction, dispersal, and consumption. The latter time is the total GMC mass divided by the galactic star formation rate. We suggest that the dispersal time is the fastest of these and is comparable to the dynamical time because star formation begins and ends quickly in a GMC. The destruction time is longer because each GMC may go through several stages of star formation following disruption in active cores. The consumption time is longest because the efficiency of star formation in each event is low and relatively little gas gets used up. GMCs exist in one place for a dispersal time and they exist as entities for a destruction time. There is no physical meaning to the consumption time as far as an individual GMC is concerned.

The fourth point mentioned above, that there are molecular diffuse clouds in the inner galaxy, follows from the fact that molecular self-shielding is independent of cloud self-gravity, depending more on the product of density and column density in the shielding layer than on any property of the cloud interior. High pressure regions have higher diffuse cloud densities in thermal equilibrium with the radiation field, and so require lower column densities for self-shielding. Thus the diffuse molecular mass can be high in high pressure regions, which includes the inner parts of galaxies and starburst galaxies (Elmegreen 1993). The observed galactic gradients in molecular fraction are partially the result of this pressure gradient combined with a metallicity gradient (Honma, Sofue & Arimoto 1995; Wong & Blitz 2002). In M64, 25% of the CO molecular mass is diffuse (Rosolowsky & Blitz 2005).

These points illustrate how the molecular mass can be high and the star formation rate low. The star formation rate is the efficiency per cloud multiplied by the cloud formation

rate, which equals the destruction rate when the total CO mass is constant. The efficiency is very low in GMCs, a few percent (Williams & McKee 1997), so the consumption time, which is the ratio of the cloud mass to the star formation rate, is long. The efficiency is low for GMCs because only a small fraction of the GMC mass is involved with active star formation. These active regions are, for example, HCN cores (Sect 3.3). In such cores the total efficiency is higher than it is in a GMC by the cloud to core mass ratio. The formation and destruction rates of HCN cores could by dynamical as well, and much faster than the CO formation and destruction rates because of the higher density. As for CO, the HCN core lifetime is the ratio of the HCN mass to the star formation rate divided by the efficiency in the HCN core. This efficiency is higher than in the CO cloud, but it still quite small because the real action happens in even denser sub-cores (e.g., the CS cores) which have an even lower total mass and a higher local efficiency (e.g., Shirley et al. 2003). Eventually a high enough density should be reached where the total galactic mass divided by the local dynamical time is within a factor of a few times the total star formation rate. There, the efficiency will be high, 30% to 50%, and the final contraction to a unique star take place. The correspondence between decreasing scale and increasing efficiency is expected for hierarchically structured clouds.

Dense, high-efficiency regions of star formation have probably been observed. The mm-wave continuum cores and other dense cores that have a Kroupa (2001) mass function show a shift in the turnover mass at some value that is higher than the stellar IMF turnover by a factor of about 3 (Motte et al. 1998; Testi & Sargent 1998; Johnstone et al. 2000, 2001; Motte et al. 2001; Beuther & Schilke 2004; Stanke et al. 2006; Alves, Lombardi & Lada 2007). If these dense cores form individual and binary stars, then their efficiencies are the inverse of this factor. This final stage has an extremely fast dynamical time compared to that in the lower density gas. The contraction can be significantly retarded by magnetic forces without affecting our proposal that cluster-forming cores (which have lower average density) evolve in a dynamical time. The bottleneck in the star formation processes is at the lower densities, where the evolution is slow because the dynamical time is long.

The historical decrease in molecular cloud lifetime that was mentioned at the beginning of this section has a simple explanation. Generally, as the scale of the region observed has decreased with improved instruments and finer surveys, the lifetimes of the clouds that are seen have dropped. Gas structure has a wide range of scales and no characteristic scale, as shown by the power law power spectra of HI (Dickey et al. 2001) and CO (Stützki et al. 1998). Surveys with particular sampling sizes tend to highlight structures with a narrow range of scales, from several times the sampling size (Verschuur 1993) to several tens of the sampling size, as which point the largest structures tend to be ignored in favor of the clumps inside these structures. That is, clusters of clumps are not found by clump-finding algorithms.

The algorithms only find continuous regions, and these are always close to the resolution limit of the telescope or survey. Because all structures evolve on their local dynamical time, higher resolution surveys that find smaller clouds also observe smaller lifetimes.

For example, giant spiral arm features ("beads on a string") that produce star complexes 300 pc in diameter remain active for $\sim 30-50$ My (Efremov 1995), GMCs that produce OB associations (which are generally inside star complexes in a hierarchical sense; e.g., Battinelli, Efremov & Magnier 1996) last $10-20$ Myr, while GMC cores that produce clusters last only ~ 3 Myr. Generally there are several generations of small-scale star formation inside each large-scale region (Efremov & Elmegreen 1998). Thus, star formation is hierarchical in time as well as space. This double hierarchy can be misleading because observations always contain selection effects. OB associations and the 10^5 $M_\odot$ GMCs that make them are not a characteristic scale for star formation even though they all have about the same size in normal galaxy disks: ~ 80 pc (Efremov 1995). They are selected for that size by the selection of a star-formation time scale through the survey requirement that O stars are still present. Once a survey is about OB associations, the size of the region is fixed by the dynamical time scale. This size will be larger in higher pressure regions because of the way size R and dynamical time scale with pressure P: $R^2/\left(t_{dyn}^4 P\right) \sim G/2.5$ (Elmegreen 1989). The associated stellar and cloudy masses will be larger in high pressure regions too: $M^2/\left(P^3 t_{dyn}^8\right) \sim 1.6G$. The same can be said for other stellar clusters selected by age, such as T-Tauri associations with smaller t_{dyn} and star complexes with larger t_{dyn}, as identified by Cepheid variables and Red supergiants (Efremov 1978). For these reasons, more recent surveys with smaller scale resolutions get shorter cloud lifetimes.

3.2. The Small Scale

An important consideration is how far down in scale the dynamical evolution goes, and whether it slows when star formation begins at the bottom. Elmegreen (2000) compiled evidence that a dynamical cascade persists down to the scale of embedded star clusters without significant delay on the small scale. The time scale for each level was said to be $\sim 1-2$ crossing times where the crossing time was taken to be $R/V \sim 1.09/\left(G\rho\right)^{1/2} \sim t_{dyn}$ for a uniform virialized cloud. For molecular density n, $t_{dyn} \equiv \left(G\rho\right)^{-1/2} = 61 n^{-1/2}$ Myr. Star formation cannot be as fast as a single crossing time or shorter than a crossing time (unless there is an implosion – Lintott et al. 2005) because turbulent and magnetic energy has to dissipate; thus 1-2 crossing times seemed to be a reasonable match to the observations. Tan, Krumholz & McKee (2006) suggested there is a delay for clusters, amounting to $\sim 4-5$ crossing times. They suggest the longer time requires near-equilibrium cloud support. Here

we review the issues raised in these papers.

The discussion in Elmegreen (2000) had four points: (1) hierarchical structure in young stars often mimics hierarchical structure in molecular clouds, implying these stars had less than a crossing time to mix, (2) embedded clusters ages are relatively small, (3) age differences between neighboring clusters are relatively small, and (4) a high fraction of dense cores contain young star formation. The case for short star formation times was independently made by Ballesteros-Paredes, Hartmann, & Vázquez-Semadini (1999), based on the short duration of star formation in Taurus. A recent review of short time scales is in Ballesteros-Paredes & Hartmann (2007).

The discussion in Tan, Krumholz, & McKee (2006) had six points: (1) CS clumps are nearly round, (2) clusters are generally smooth, (3) protostellar wind momentum, which is proportional to the star formation rate, is small, (4) cluster age spreads are relatively large, (5) a dynamical ejection event in the Orion Nebula cluster occurred a relatively long time ago (2.5 Myr), and (6) stellar mass segregation requires a relatively long time. The third method using wind momentum is highly inaccurate, as these authors admit, so we will not use it here to determine a cluster formation time to within the desired factor of 3.

The other points are reconsidered here. We begin with the usual caution that star forming regions have a range of densities so the crossing time does not have a single value. The dynamical time will also be longer for the lower density regions, so the total age spread for stars should be larger than the age spread in a cluster core. As clouds contract and the density increases, the crossing time decreases, so prior star formation in the same cloud will have a longer time scale than current star formation in the core (we show a model of this in Sect. 3.4). Thus, fairly old stars should always be present in an active region even if the current level of activity is short-lived. Palla & Stahler (2000) have termed this evolution accelerated star formation: the star formation rate in a region increases with time until the final cloud core is disrupted. Huff & Stahler (2006) found an extended age distribution in the Orion Nebula cluster and modeled it with continuous star formation during monotonic cloud collapse. There was no equilibrium or energy feedback in their model and yet the evolutionary time scale matched the stellar ages. For these reasons, we do not consider the observation of relatively old stars or relatively old ejection events to be an indication that cloud cores are stable. This point is relevant to some of the discussion in Tan, Krumholz, & McKee (2006), and also counters most of the discussion in Tassis & Mouschovias (2004).

There remain two lifetime indicators that are based on morphology alone: clump shapes and cluster substructure. Tan, Krumholz & McKee (2006) note that CS cores forming high mass stars are circular to within $\sim 26\%$. Equilibrium clouds are also round so they conclude the CS clouds are in equilibrium. However, numerical simulations form roundish objects

that are not in equilibrium (Ballesteros-Paredes & Mac Low 2002; Gammie et al. 2003; Li, et al. 2004), and other cores are more irregular than the CS observations suggest (Myers et al. 1991; Bacmann et al. 2000; Steinacker et al. 2005). The CS sources cited by Tan, Krumholz & McKee were observed by Shirley et al. (2003) with a 24.5 arcsec beam at an average distance of 5.3 kpc, making the average beam half-size 0.31 pc. The average deconvolved radius of a CS core was calculated to be 0.37 pc, which is about the same. Thus the sources are barely resolved. The major and minor axes used by Shirley et al. to obtain the average ellipticity measurement of 1.26 did not consider deconvolved beams, however, so the intrinsic ellipticity ratios are higher than the observed ratios. Higher resolution observations may eventually show irregular substructures like those commonly seen at lower densities; then the CS cores would appear to be more rapidly evolving.

Cluster substructure consists of stellar hierarchies and filaments that mimic cloud hierarchies and filaments (Gomez et al. 1993; Testi et al. 2000; Heydari-Malayeri et al. 2001; Nanda Kumar, Kamath, & Davis 2004; Smith et al. 2005; Gutermuth et al. 2005; Stanke, et al. 2006; see review in Allen et al. 2006). The clusters have to be fairly young to show it, and even then it appears most prominently in the youngest protostars (e.g., Dahm & Simon 2005). By the time a cluster core is ready for disruption, which may be 1.5 crossing times after its most active phase began, the oldest stars will have moved around enough to mix their birth sites and only the pre-stellar cores and youngest protostars will still show gas-like morphologies.

The discussion about this in Section 2.2 of Tan, Krumholz, & McKee (2006) has a different conclusion. They consider a cluster mass M forming in a total time t_{form}, and a total mass in subclusters, M_{sub}, which each form and disperse in a time t_{dyn}. For unbound subclusters, the steady state gives $t_{form} = (M/M_{sub})\, t_{dyn}$. For bound subclusters, they consider the individual lifetimes to be the time for a subcluster to sink to the cluster center by dynamical relaxation, which is $\sim 0.17\Lambda \ln \Lambda$ dynamical times for Λ equal to the ratio of the cluster mass to the mass of an individual substructure. For IC 348, which has 8 subclusters with 10-20 stars each out of the total of 345 stars, the unbound case gives $t_{form} \sim 5 t_{dyn}$ and the bound case in their analysis gives $t_{form} \sim 21 t_{dyn}$. We note that t_{dyn} for the unbound case was assumed to be the dynamical time for the substructure, which is less than the dynamical time for the larger-scale core according to the usual time-size-velocity scaling relation. For example, if the substructure is 1/4 of the core size and the dynamical time scales with the square root of size as in the Larson (1981) law, then t_{form} would be only $2.5 t_{dyn}$ in the unbound case. However, the basic model should be questioned. Bound and unbound substructures should interact with each other more frequently than they evolve on their own. A substructure with any reasonable size cannot cross from one side of the cloud core to the other without mixing with another substructure. Colliding loose substructures

either merge or destroy each other if their collision speed is less than a few times their internal dispersion (e.g., Aarseth & Lecar 1975). Their lives are much shorter than either their own dissolution time or their sinking time from dynamical friction. For example, the filamentary structures seen in young mm-wave continuum sources and the hierarchical structure seen in young stars and protostars have characteristic outer scales that are comparable to the scales of the cluster cores. If stars are born with the same pervasive hierarchy as the gas, which extends over all available scales, then each subcluster can hardly move without interacting with another one. Only the smallest and densest might last for a full crossing time. Thus clusters substructure should be evanescent with average individual lifetimes much less than a core crossing time. This short time accounts for the low fraction of clusters with substructure even when the star formation time is only 1-2 crossing times.

Krumholz & Tan (2007) continue the discussion of relatively long time scales by comparing the star formation efficiency per unit free fall time, ϵ_{ff}, for a variety of molecular tracers. The free fall time is $t_{ff} = (3\pi/32G\rho)^{1/2}$, which is $(3\pi/32)^{1/2} = 0.54$ times the crossing time, so a star formation efficiency of 1% in a free fall time corresponds to a star formation efficiency of 1.8% in a crossing time. They suggest the average ϵ_{ff} is only a few percent, independent of density, and so cluster formation with a final ~ 10 percent efficiency requires ~ 5 free fall times. There are several points to make here. First, the observed total efficiency for whole OB associations is only a few percent per generation (Williams & McKee 1997), so ~ 1.5 free fall times in a GMC ($= 0.75$ crossing times) is a reasonable result for these large scales, and it requires the GMC evolution time to be short as suggested here. Second, a slight increase in ϵ_{ff} with ρ in Figure 5 of Krumholz & Tan (2007) was not mentioned but it might be expected for several reasons. In the Krumholz & McKee (2005) model, ϵ_{ff} scales with the inverse cube root of Mach number (their eq. 30), and the Mach number could decrease for higher density regions. If we consider the Larson (1981) correlations as Krumholz & McKee do, in which the linewidth scales approximately as $\rho^{-1/2}$, then the inverse cube root of Mach number scales with $\rho^{1/6}$ for a constant temperature, and this is about the trend in ϵ_{ff} with ρ in Krumholz & Tan (2007). On the other hand, the linewidth-density relation in Plume et al. (1997) goes the opposite way for dense gas, $\Delta v \propto \rho^{0.3}$, and then ϵ_{ff} would not increase with ρ if $\epsilon_{ff} \propto \Delta v^{-0.3}$ from the Krumholz & McKee theory. On a more general level, an increase in ϵ_{ff} with ρ should be expected regardless of the dynamics for hierarchically structured clouds, because the mass fraction of dense star-forming clumps always increases with the average density (Elmegreen 2005). This is what the observations in Krumholz & Tan show most directly, and it does not support or refute any particular model of star formation.

The highest-density value for ϵ_{ff} in Krumholz & Tan (2007) comes from CS emission, and these authors suggest it is overestimated by a factor of a few because of undersampling in the CS surveys by Plume et al. (1997) and Shirley et al. (2003), who observed only

H_2O maser sources. Krumholz & Tan assume $L_{CS} > 20$ $L_\odot$ from Plume et al., derive a conversion of $M_{CS}/M_\odot = 4.5 \times 10^4 L_{CS}/L_\odot$, and get a CS mass limit of $> 9 \times 10^4$ $M_\odot$. This is divided by a star formation rate of 3 $M_\odot$ yr^{-1} and by the free fall rate at the beam-diluted average CS density of 1.8×10^5 cm^{-3} to get $\epsilon_{ff} < 0.27$. Shirley et al. (2003), however, state that $L_{CS(5-4)} = 20$ $L_\odot$ is the most likely value for the Milky Way after considering various completeness corrections, so the Krumhjolz & Tan value of ϵ_{ff} may not be so high. Even so, with a factor of 3 downward correction for L_{CS}, the $\epsilon_{ff} - \rho$ correlation in Krumholz & Tan is still present because the plotted CS point is 10 times higher than the others at the same density. More important to the present paper is the observation in Plume et al. and Shirley et al. that the ratio of bolometric luminosity to virial mass in CS gas is a factor of several hundred higher than in CO gas, and also relatively constant from region to region spanning a factor of 100 in gas mass. Thus the CS gas is closer to the star formation stage than CO. The efficiency should increase in this way with density as the observations zero-in on the individual star-forming cores. This takes us back to the fundamental property of hierarchical clouds mentioned above, that the mass fraction of the densest cores increases with the average density.

The most peculiar point in the Krumholz & Tan diagram is the low value for HCN, which has $\epsilon_{ff} \sim 0.0058$. This is lower than the other values at the same density by a factor of ~ 10 and the corresponding long time for HCN evolution could raise questions about the time scale for star formation. We discuss this HCN value now.

3.3. The Evolution Time in HCN Cores

Gao & Solomon (2004a,b) and Wu, Evans, et al. (2005) derived the star formation rate in HCN clouds using the associated IR luminosity. They observed the proportion $L_{IR} \sim 900 L_{HCN}$ $L_\odot \left(\mathrm{K\ km\ s^{-1} pc^2}\right)^{-1}$, and then converted the L_{IR} to a star formation rate with $\dot{M} = 2 \times 10^{-10} \left(L_{IR}/L_\odot\right)$ $M_\odot$ yr^{-1} from Kennicutt (1998). They converted L_{HCN} to a mass using the virial theorem, $M_{dense} = \alpha L_{HCN}$ with $\alpha \sim 10$ $M_\odot$ $\left(\mathrm{K\ km\ s^{-1} pc^2}\right)^{-1}$. As a result, the time scale is

$$\frac{M_{dense}}{\dot{M}} = \left(\frac{M_{dense}}{L_{HCN}}\right)\left(\frac{L_{HCN}}{L_{IR}}\right)\left(\frac{L_{IR}}{\dot{M}}\right) \sim 5.5 \times 10^7 \text{ yrs}, \quad (1)$$

which is much longer than the dynamical time at the high density of HCN. The virial theorem conversion factor comes from the equations $M = 5R\Delta v^2/G$ and $L_{HCN} = T\left(8 \ln 2\right)^{1/2} \Delta v \pi R^2$ for Gaussian dispersion of the emission line Δv and source radius R. These equations give $\alpha = 2.1 n(H_2)^{1/2}/T$ for density $n(H_2) = 3M/\left(4\pi R^3 m(H_2)\right)$. HCN requires excitation at $n = 3 \times 10^4$ cm^{-3} and Gao & Solomon assume $T = 35$K, which gives $\alpha = 10$ as above.

Gao & Solomon (2004a,b) observed unresolved HCN emission from whole galaxies, while Wu et al. (2005) observed individual star-forming regions in the Milky Way. The $L_{IR}-L_{HCN}$ correlation was about the same for each, and this is a bit surprising. In whole galaxies, the IR comes from massive stars whether they are inside or outside the dense neutral cores, whereas the HCN comes only from the cores. Generally O-type stars disperse their cores and break out quickly, long before they supernova. The time spent inside a core, which is the star formation timescale of interest for this paper, can be arbitrarily short for the same total L_{IR}, M_{dense} and $\dot{M}$. For example, an O-type star might spend its first 0.2 Myr inside an HCN core before disrupting it and then spend the remainder of its 3 Myr lifetime outside HCN cores. Then the star formation rate in a core is 3/0.2 time the average rate, and the HCN timescale per core is 0.2/3 of 55 Myr, or 3.7 Myr. Correspondingly, 0.2/3 = 6.7% of O-type stars would be in HCN cores at any one time. Clearly for whole galaxies, the HCN timescale derived above is not equivalent to the duration of star formation inside an HCN core.

The situation for individual star-forming regions is different. All of the points in Figure 5 of Krumholz & Tan (2007) other than HCN were for individual regions, as was the Wu et al. (2005) contribution to the HCN point. In this case, the duration of star formation in an HCN core equals the efficiency of star formation there multiplied by $M_{dense}/\dot{M}$, and this product can be much less than $M_{dense}/\dot{M}$ alone. The average efficiency of star formation in a dense core is half the final efficiency if stars form with a uniform rate, and the final efficiency is probably only $\sim$ 10%, considering that $\sim$ 90% of embedded clusters become unbound after the gas leaves (which requires a low final efficiency and rapid gas clearing; Lada & Lada 2003). Thus the average efficiency during the embedded lifetime may be only $\sim$ 5%, in which case the duration of star formation in HCN cores is $0.05 \times 55 = 2.75$ Myr. If star formation accelerates in a cloud core (Palla & Stahler 2000), then the average stellar mass fraction during the lifetime of the core is less than half of the final mass fraction, and the core duration would be less than 2.75 Myr.

The duration of star formation in HCN cores should be the same everywhere because HCN excitation corresponds to a certain density and the dynamical time at that density is fixed. Thus the agreement between the Gao & Solomon correlation and the Wu et al. correlation begins with a fundamental timescale that is the same for each and then multiplies this timescale upward by about the same amount for each. The multiplication factor for the galactic scale is the inverse of the fractional time that O-type stars spend in HCN cores. For smaller scales, it is the inverse of the average star formation efficiency in an HCN core. These factors may not be exactly the same, but for the 9 orders of magnitude in L_{IR} separating the Gao & Solomon results from the Wu et al. results, differences in the conversion factors amounting to a factor of $\sim$ 3 will not be noticed.

The lifetime of the HCN gas (55 Myr) still has to be explained. This lifetime is much longer than a crossing time and in this sense faces the same problem as the CO-emitting gas in the Zuckerman & Evans (1974) discussion. The solutions could be similar too. First, the HCN cores as a whole should evolve more slowly than their denser subcores where the stars actually form, so the HCN stage prior to star formation should be slower than the stage after star formation in a sub-core becomes disruptive. Second, HCN should be only partially converted into stars during cluster formation (the low efficiency) and the residual should be pushed aside at high pressure without decreasing its density much. Then it stays HCN but has a geometry temporarily unsuitable for star formation until it recollapses in a different position later. Third, some HCN is probably not in the form of strongly self-gravitating cores where individual stars form, but is diffuse intercore gas that is at a high enough density and opacity to excite HCN. In this sense, HCN alone, like CO alone, is not the star-forming gas but provides an envelope or intercore matrix to the star-forming gas, which is much denser. Of all these, the low efficiency in each HCN core, discussed above, is probably the dominant cause of the relatively long consumption time.

High resolution observations of HCN regions should show a low fraction of the gas actively involved with star formation, as do observations of CO clouds. However, it may be that nearly every HCN region still contains some star formation, which is the case for CO too. The inactive HCN, like the inactive CO, should be peripheral or intercore gas in the immediate vicinity of star formation, and it should not be strongly self-gravitating by itself. Dense self-gravitating cores in the same regions are the more likely precursors of young stars, and their contribution to the HCN mass fraction should be low, like the 5-10% estimated above. There should also be evidence for HCN mini-shells, comets, and other disturbances at these high densities. These should resemble structures observed on much larger scales in CO. Their presence would indicate that cloud core dispersal maintains a high density for a crossing time while second generations of stars might be triggered into forming.

CS-emitting gas is closer to the density where star formation becomes highly efficient, and the consumption timescale for CS is correspondingly shorter than for HCN. Plume et al. (1997) estimate this timescale is 13 Myr based on the total CS mass divided by the Galactic star formation rate. This is still much longer than the CS crossing time (0.12 Myr), so the CS abundance has the same problem as HCN and CO with probably the same solution: it either has to recycle after discrete events or form stars in a small fraction of its mass (sub-cores) where the local efficiency is higher.

3.4. The Huff & Stahler Accelerated Star Formation Model with Feedback

Huff & Stahler (2006) observed the history of star formation in the Orion Nebula cluster and found accelerated star formation with some stars older than the current crossing time. They suggested a model of cloud evolution where energy dissipation removes turbulent support and the cloud contracts, slowly at first, and then faster as the dissipation and dynamical times get shorter. Their model has no stellar energy input or feedback and still the cloud evolves relatively slowly because it takes time to dissipate the turbulent energy. Cloud contraction also generates more turbulent energy from the change in PdV for boundary pressure P and volume V. This model is useful as a starting point to investigate star formation in cores when feedback is added. To do this, we begin with the Huff & Stahler evolution equation for a singular isothermal sphere and add an energy input term that is a function of the stellar mass

$$\frac{dH}{dt} = -\eta \frac{M_{cloud} v^3}{2R} + \Gamma M_{star}^{\gamma}, \tag{2}$$

where M_{cloud} is constant, M_{star} is the increasing stellar mass, v is the velocity dispersion, R is the radius, and H is the enthalpy. The power γ depends on the types of stars that form. For a massive cluster where O-type stars form, γ is large because the luminosity, particularly beyond the Lyman continuum, is a sensitive function of stellar mass. For a low mass cluster or for a cluster where ionization is not important, $\gamma \sim 1$. We consider both cases here. Figure 1 shows the Lyman continuum luminosity (bottom) and the total luminosity (top) as functions of the cluster mass. These curves were obtained by randomly sampling the IMF until the desired cluster mass was achieved. The IMF ranges from 0.01 $M_\odot$ to 150 $M_\odot$ with a flat slope below 0.5 $M_\odot$ and a slope of -1.5 above that, for logarithmic mass bins (where the Salpeter slope is -1.35). Each cluster mass used 1000 random trials and took the resulting average luminosity. The rms variations around these luminosities are shown by dashed lines using the right-hand axes. The stellar luminosities and masses were obtained from Vacca, Garmany, & Shull (1996). The top panel shows that the total luminosity increases approximately in proportion to the cluster mass because the luminosity is heavily weighted by low mass stars. The Lyman continuum luminosity is strongly dependent on cluster mass ($\gamma \sim 40$ in places), with a sudden turn on of the Lyman continuum flux at $M_{cluster} \sim 10^3$ $M_\odot$, where O-type stars first begin to appear. In the following models, we take $\gamma = 1$ and 2 to illustrate the main points.

The kinetic energy in an expanding HII is approximately independent of time and depends mostly on the initial thermal energy in the HII region provided by the ionizing flux. This follows from the expansion equation $R = R_0 \left(1 + 7 a_{II} t / 4 R_0\right)^{4/7}$, which gives a velocity-squared proportional to $R^{-3/2}$, and from the HII region mass, which is $M = (4\pi/3) m_H n R^3$ for

$(4\pi/3)nR^3 = ([4\pi/3]SR^3/\alpha)^{1/2}$. Here S is the Lyman continuum flux, α is the recombination coefficient to the second level of hydrogen, n is the HII region density, and R is the HII region radius. The radius-dependence for mass and velocity-squared cancel, leaving the expansion kinetic energy constant at approximately its initial thermal value, $0.5M_0a_{II}^2$, where M_0 is the Stromgren sphere mass at the initial cloud density and a_{II} is the thermal speed in the HII region. The kinetic energy therefore depends on the square root of the Lyman continuum flux. This justifies the use of this flux as a crude measure of cloud-core destruction rates.

The stellar mass in our adaptation of the Huff & Stahler model comes from the volume and time integral over the instantaneous star formation rate, which is taken to be $\epsilon_{cr}\rho\left(G\rho\right)^{1/2}$ for constant efficiency per crossing time ϵ_{cr}. The volume integral gives

$$\frac{dM_{star}}{dt} = \epsilon_{cr}\int_{R_{min}}^{R_0}\rho\left(G\rho\right)^{1/2}4\pi R^2 dR = \epsilon_{cr}\left(\frac{GM_{cloud}^3}{4\pi}\right)^{1/2}\frac{\ln\left(R_0/R_{min}\right)}{R_0^{3/2}} \tag{3}$$

for a singular isothermal sphere with $\rho(R) = \rho_0\left(R_0/R\right)^2$ (as assumed by Huff & Stahler 2006). The collapse is assumed to decrease R_0 while keeping the total cloud mass constant. The log term has assumed a minimum radius, or inner core radius, R_{min}, to terminate the singularity. The enthalpy is $H = -GM_{cloud}^2/\left(12R\right)$ (Huff & Stahler). The energy dissipation rate is assumed to be $-\eta v^3/\left(2R\right)$ from Mac Low (1999), who determine $\eta \sim 0.4$. We take $\eta = 0.3$ here to be slightly conservative (small values lengthen the contraction and star formation time scales relative to the crossing time). We also take $\epsilon_{cr} = 0.1$ and three values of Γ for each case to give a reasonable range for the final mass of stars. The equations are integrated numerically over time.

Figures 2-4 show the results. In Figures 2 and 3, $\gamma = 1$ and the cloud mass is 10^3 $M_\odot$ and 10^4 $M_\odot$, respectively. In Figure 4, $\gamma = 2$ and the cloud mass is 10^4 $M_\odot$. The starting radii are $R(t = 0) = 3$ pc for the first case and 6 pc for the second two cases; $R_{min} = 0.1$ pc. In the bottom panels, the radius, stellar mass, and star formation rate are plotted versus the absolute time, and in the top panels these quantities are plotted versus the relative time, which is the absolute time divided by the instantaneous dynamical time, $(G\rho)^{-1/2}$. The different values of Γ are plotted in separate curves, as indicated. In each case, the radius decreases at first, as in the Huff-Stahler solution, because there are few young stars to add turbulent energy. When the density and star formation rate reach a sufficiently high value, the energy input rate from stars begins to exceed the turbulent energy loss rate and the radius increases. Then star formation slows down because of the decreasing density. Lower Γ cases produce higher stellar masses.

The duration of the most active phase, which is taken to be the full width at half maximum in the lower middle panel of Figures 2 to 4, is only several instantaneous crossing

times even if the age range in the cluster is many instantaneous crossing times and a large total value in absolute time. In Figure 2, for example, the width of the highest star formation peak is ~ 5.3 Myr, which is ~ 1.4 times the age at the peak. In the top middle panel the age at the peak is 1.8 instantaneous crossing times. Multiplying the relative time by the fractional total time gives 2.5 crossing times measured at the peak density for the FWHM duration of star formation. The relative durations of all three curves are given in the top middle panel in order of decreasing Γ. Figures 3 and 4 also give the relative durations. For these two cases, the lowest Γ has unrealistically strong star formation because the final efficiencies exceed 60%; the middle Γ are best, giving $\sim 30\%$ efficiency. The corresponding FWHM durations of star formation are 1.8 and 1.6 crossing times at peak density. In terms of absolute time, there are old stars present dating back to when the cluster was young, which can be several million years. The case closest to a massive dense cluster like 30 Dor is in Figure 4 with $\Gamma = 0.0026$, for which a 10^4 $M_\odot$ cloud produces a $\sim 3 \times 10^3$ $M_\odot$ cluster in a burst lasting 2.6 Myr and 1.6 crossing times at the highest density.

This example is a crude model for the formation and disruption of a cluster, but it illustrates the point also made in sections 3.1 and 3.2 that star formation can be fast in terms of the instantaneous dynamical time, even though the absolute rate varies from slow at the beginning, to fast in the densest phase, to slow again after the disruption.

A second conclusion to be made from this analysis is that the conceptual difference between star formation rate and instantaneous luminosity is important. The luminosity is not proportional to the star formation rate but to the integral of the star formation rate over time. So any point in the evolution where the stellar disruptive luminosity balances the turbulent dissipation rate is quickly passed as stars continue form. There is no stable state because stars keep forming and the luminosity keeps increasing even when there is a temporary equilibrium. Vázquez-Semadeni et al. (2005) and Bonnell & Bate (2006) also note the lack of stable equilibria in cluster-forming cores.

Li & Nakamura (2006) and Nakamura & Li (2007) took a different approach. They ran realistic MHD simulations (although without magnetic diffusion) that generate quasi-stable equilibria through protostellar wind feedback. The latter paper gets a star formation rate of a few percent of the cloud mass in each free fall time and it maintains this rate for 1.5 initial free fall times ($t_{ff} = 1.2$ Myr). The equilibrium state is maintained for the last one free fall time, although it may have been able to continue longer if the code ran longer. After $1.5t_{ff}$, 80 stars formed. This model is like the one shown in Figure 2 in the sense that it is a low mass cloud ($\sim 10^3$ $M_\odot$) without ionization. In Figure 2, the duration of star formation is also about 1.5 instantaneous free fall times, although there is no equilibrium. This distinction between models raises an important point. In our figures, the collapse turns

around because of intense stellar pressures at some high density, where the star formation rate is high. Viewed in a narrow time interval around this turning point, one dynamical time wide, there is an equilibrium. However, stars continue to form and the balance of forces continues to build in favor of cloud dispersal. Soon the cloud expands and star formation slows down. This all happens in less than a few crossing times. The same turnaround might happen in the Nakamura & Li models: as stars continue to form, their collective winds and radiation should continue to agitate the gas and eventually overcome the total dissipation rate, which is somewhat fixed for a constant average density and Mach number. Their simulated cloud should then expand and the star formation rate should decrease. It would seem to take some tuning to maintain an equilibrium for much longer than 2 to 4 t_{ff} because the collective effects of winds and radiation should then be quite influential. One way to tune the result would be to turn off the winds after a short time in each star. A second point of comparison is that for most of the present paper we are concerned with massive clusters, and then ionization destroys and displaces a high fraction of the core gas soon after an O-type star forms. Nakamura & Li do not consider this type of energy input, and even our models in Figure 4 do not have a high enough γ to fully account for the sensitivity of energy input to the presence of massive stars.

Another important effect might be the lack of magnetic diffusion in the Nakamura & Li (2007) models (their earlier, 2D, simulations had magnetic diffusion). Without magnetic diffusion, there is no possibility of rapid compression-induced triggering, which is an effect described in their earlier papers and studied again in Section 3.5 below. Star formation triggered by compression near the outflows could increase the efficiency per free fall time considerably and lower the overall timescale of the active phase. It could even remove the impression that there is a quasi-equilibrium if the phase of gravity/wind force balance becomes short-lived. Such wind-induced triggerings have apparently been observed (Barsony 2007). In addition, even in their paper with magnetic diffusion, Nakamura & Li (2005) do not consider the accelerated collapse that might arise from magnetic diffusion rates proportional to a power of the density greater than 0.5 (Sect. 3.6).

Krumholz, Matzner & McKee (2006) developed a detailed analytical model of cluster formation with essentially the same results as shown here, although their conclusions differed. They considered spherical self-gravitating clouds with energy input from ionization by massive stars. Each generation of star formation in their model is rapid when measured on a dynamical timescale. Their figures show oscillations on timescales of 0.5-1 crossing times, and each oscillation is a generation of stars. Thus their model agrees with the short timescale for star formation and cloud disruption discussed in the present paper. However, their model allows the energized debris from one generation to recollect at the same position and make more stars later (because everything is spherically symmetric). Real GMCs are

more filamentary (e.g., Koda et al. 2006) and star formation at one location cannot easily influence GMC turbulence or support at a distant point in the same cloud. Instead, star formation pushes on the gas in its immediate neighborhood, causing that part of the envelope to move aside, and at the same time it triggers new star formation in the compressed region (triggering was not included in their model). Recall that our application of the Huff & Stahler (2006) model was only for cloud cores of modest total mass, not for whole GMCs. Cloud cores are spherical and somewhat easily disrupted by a single star formation event, as shown in Section 3.4, while GMCs are elongated with remote parts that are not so easily disrupted by the same event.

Krumholz, Matzner, & McKee also assume that energy from each generation of star formation affects all of the GMC mass at once, and through continuous boom and bust oscillations, the total lifetime of the cloud can be extended. Our view is different. GMCs show only localized disruption from massive clusters, involving primarily the core mass ($\sim 10^4$ $M_\odot$) and some triggering in nearby parts of the cloud, with slow and quiescent star formation elsewhere. Something other than star formation has to support the remote diffuse parts, and observations suggest this is a combination of modest turbulence with a strong (sub-critical) magnetic field (e.g., Cortes, Crutcher, & Watson 2005). This is the standard model as far as the low-density envelope is concerned.

Our primary point about rapid star formation is that a whole cloud begins star formation rapidly somewhere inside of it, and that part ends star formation rapidly as well. This is unlike the standard model, which would introduce a delay everywhere of some $10t_{dyn}$ because of slow ambipolar diffusion. For the star-forming part of the cloud, we agree with the rapid timescale of the Huff & Stahler (2006) model. For the rest of the cloud, we agree with the longer timescale of the Mouschovias (1991) model, provided it is recognized that the cloud moves around every few crossing times because of pressure from star-forming cores. Further discussion on long-term cloud evolution is in Section 4.

3.5. Turbulence Compression and Enhanced Magnetic Diffusion in Cloud Envelopes

Turbulent fragmentation as a model for star formation (see review in Mac Low & Klessen 2004) applies best to cloudy regions that are not collapsing already. Once collapse begins, the dynamics of the collapse takes over using the initial conditions from the turbulent state (e.g., power-law power-spectrum of velocities, with hierarchical filaments and clumps; Li et al. 2004; Bate & Bonnell 2005; Jappsen et al. 2005; Tilley & Pudritz 2005; Martel et al. 2006). Turbulent fragmentation was originally envisioned as a way to get high densities

inside clouds, considering that star formation is more rapid in the compressed regions than in the cloud as a whole. Another aspect is also important, and that is the enhanced expulsion of magnetic flux from the compressed gas (e.g., Nakamura & Li 2005; Kudoh & Basu 2007). The point is that slow ambipolar diffusion at the low average density of a cloud or GMC envelope is not relevant for star formation. Diffusion is relatively fast in the clumps where stars actually form.

Compression enhances diffusion by changing the force density balance in a magnetically critical cloud from one where $g\rho \sim B^2/(4\pi R) \sim \rho n_i \alpha_{in} R \omega_{diff}$ for gravitational acceleration $g \sim G\rho R$ and cloud radius R, to one where $g_c \rho_c < B_c^2/(4\pi L) \sim \rho_c n_{i,c} \alpha_{in} L \omega_{diff,c}$ in the clumps. Subscript c represents the compressed clump state, L is the compressed clump size, and ω_{diff} is the magnetic diffusion rate. Self-gravity is written here as relatively unimportant during the initial compression, although this would not always be the case. Writing the clump ionization fraction as $x_c = n_{i,c} m/\rho_c$ for mean molecular weight m, we get a magnetic diffusion rate

$$\omega_{diff,c} = \frac{B_c^2 m}{(\rho_c L)^2 x_c \alpha_{in}}. \tag{4}$$

The column density does not change much with fast lateral compression ($\rho R \sim \rho_c L$) but the field strength does, by flux freezing, as $B_c \sim B\,(R/L)$, thus

$$\frac{\omega_{diff,c}}{\omega_{diff}} \sim \frac{R^2 x}{L^2 x_c} >> 1. \tag{5}$$

This enhancement factor for the diffusion rate is larger than the time factor during which the turbulence-compressed state is maintained, so there is a net flux loss from the clump. The duration of the pre-compressed state is $\tau = R/v_A$ for Alfvén speed $v_A = B/(4\pi\rho)^{1/2}$ initially comparable to the virial speed $(gR)^{1/2}$. The duration of the compressed state is $\tau_c = L/v_{A,c}$ where $v_{A,c} \sim v_A\,(R/L)^{1/2}$. Thus the ratio of durations is $\tau_c/\tau = (L/R)^{3/2}$. Multiplying this by the ratio of diffusion rates, we get the relative enhancement of flux loss as

$$\frac{\omega_{diff,c}\tau_c}{\omega_{diff}\tau} \sim \frac{R^{1/2} x}{L^{1/2} x_c} \sim \left(\frac{R}{L}\right)^{0.5+\kappa} >> 1 \tag{6}$$

for ionization fraction varying with density as $x \sim n^{-\kappa}$ and n inversely proportional to size during the compression. In simulations by Nakamura & Li (2005), $\kappa \sim 0.5$ and they find enhanced flux loss. The compression-induced flux loss is larger if $\kappa \sim 1$ in the dense state, as suggested in the Section 3.6.

For a magnetically critical cloud, $\tau \sim t_{dyn}$ and $\omega_{diff}\tau \sim t_{dyn}/t_{diff} \sim 1/10$. If $(R/L)^{0.5+\kappa} > 10$, which is reasonable, then $\omega_{diff,c}\tau_c > 1$ and the clump diffusion time is less than the duration of the compressed state. This means that a high fraction of the magnetic flux will

diffuse out. In this case, turbulence compression not only makes the dense regions but it also forces so much magnetic flux from them that they can become supercritical in a crossing time and collapse quickly into stars. This triggering process is much faster than the same gas would have evolved on its own from an initially sub-critical state.

The regions where turbulence-enhanced compression and diffusion should be important include marginally stable GMCs envelopes and non-collapsing central regions, in addition to diffuse and low-pressure molecular regions that are sub-critical on average. Compression-enhanced diffusion should also be important in GMC envelopes where HII regions and other pressures trigger star formation. The compression has to be strong enough ($R >> L$) to make $\omega_{diff,c}\tau_c > 1$. We consider in Section 5 whether the IMF should be different in turbulence-compressed regions than in collapsing supercritical cores, and possibly different again for star formation that follows the standard model of slow ambipolar diffusion before collapse.

3.6. Enhanced Magnetic Diffusion in Cloud Cores

Microscopic changes should also play an important role in the rapid collapse of GMC cores, and they should aid with accelerated diffusion in the turbulence-compressed clumps of GMC envelopes. An essential consideration is how rapidly the ratio of the magnetic diffusion time to the dynamical time decreases at higher density. For typical cosmic ray ionization rates, the density scaling for the electron fraction changes from $x \propto n^{-1/2}$ to n^{-1} when charge exchange replaces dissociative recombination for the neutralization of ionic molecules, and electron recombination on neutral grains replaces dissociative recombination with ionic molecules (Elmegreen 1979; Draine & Sutin 1987). For cosmic ray ionization rates typical of the solar neighborhood, this change occurs at $n \sim 10^5$ cm^{-3}. The density scaling is important because the ratio of the diffusion time to the dynamical time drops faster for steeper scaling laws. For example, Basu & Mouschovias (1995) showed that dynamical evolution is faster when $x \sim n^{-2/3}$ than when $x \propto n^{-1/2}$. Hujeirat, Camenzind, & Yorke (2000) considered various density dependencies and found that if the power exceeds 2/3, the time for an initially subcritical core to start collapsing dynamically is equal to the initial free fall time. The $n^{-1/2}$ to n^{-1} scaling transition at $n \sim 10^5$ cm^{-3} is shown in Figure 1 of Elmegreen (1979) and in Figures 1-6 of Umebayashi & Nakano (1990).

Also at high density, the waves generated by cosmic ray streaming instabilities damp faster than their growth rate and cosmic rays stream freely along the field lines. The cosmic ray density drops sharply at this point. This drop is shown in Figure 1 of Padoan & Scalo (2005), where for dark cores it also occurs at a density of $\sim 10^5$ cm^{-3}. A sudden drop in

the cosmic ray ionization rate inside the dense parts of clouds would lead to an even greater drop in the ionization fraction.

Further loss of magnetic support at this density should arise because of changes in the grain population. Charged grains contribute substantially to the magnetic support of neutral molecules, and small grains dominate the viscous cross section. However, observations suggest that PAH molecules and small grains disappear in very dense clouds (Boulanger, et al. 1990). Depletion could cause small grains to grow. Omont (1986) suggests the depletion time onto grains is $10^{10}/n$ years, which is smaller than the dynamical time, $(G\rho)^{-1/2}$, when $n > 3 \times 10^4$ cm^{-3}. Depletion also removes ionic metals which lowers the ionization fraction. Also at about this density, grain coagulation reduces the number of charged grains and this too reduces grain coupling to neutrals (Flower, Pineau des Forêts, & Walmsley 2005). Further coupling loss arises because large grains lose their field line attachment (Kamaya & Nishi 2000). All of these microscopic effects speed up star formation at $n \sim 10^5$ cm^{-3} for Solar neighborhood conditions by allowing the magnetic field to leave the neutral gas more quickly. Only a few of these effects have been included in MHD simulations.

3.7. Slow Protostellar Motions in Rapidly Evolving Clouds

Newborn protostars that form in magnetic turbulent gas should move slower than the virial speed for two reasons. First, the magnetic field provides some support to the cloud, so most of the gas moves at sub-virial speeds anyway. Second, protostars that form in turbulence-shocked regions will have the average speed of the two colliding streams; the component of the velocity perpendicular to the shock will cancel. If magnetic energy, turbulence and self-gravity have comparable energy densities, then the turbulent speed is $(1/2)^{1/2}$ of the virial speed. Colliding flows reduce the final protostar speed by another factor of $(2/3)^{1/2}$, on average, so the net reduction is a factor of $(1/3)^{1/2} = 0.58$. Thus protostars should appear to be moving relatively slowly. Observations by Belloche, André, & Motte (2001), Di Francesco, André & Myers (2004), Walsh, Myers & Burton (2004), Jørgensen et al. (2007) and Walsh et al. (2007) show slow motions for pre-stellar cores.

The slow birth motion of pre-stellar cores implies that the protostars they eventually make will be subvirial and sink to the center of the cloud, increasing the star-to-gas mass fraction there and decreasing the required total efficiency for cluster self-binding (Elmegreen & Clemens 1985; Pinto 1987). Patel & Pudritz (1994) proposed that the cold stellar component in an embedded cluster would collapse inside the gaseous component by a two-fluid instability. If the initial protostar speed is v_i and the virial speed is v_v, then the formation efficiency that produces a 50% stellar mass fraction after protostar settling is $0.5 \exp\left(-0.75\left[1 - v_i^2/v_v^2\right]\right)$

for an isothermal cloud (Verschueren 1990). The formation efficiency for cluster binding with instantaneous gas removal is therefore 50% for $v_i = v_v$ and 30% for $v_i = 0.58 v_v$. It is smaller for slow gas removal (Lada, Margulis, Dearborn 1984), and smaller still if some stars escape leaving a tighter cluster in the core (Boily & Kroupa 2003).

Before a pre-stellar clump detaches from the magnetic field on which it formed, its motion will be influenced by the magnetic field. If the magnetic field in a protostellar clump is critical, or if the clump forms with a constant mass-to-flux ratio in a cloud where the average magnetic field is critical, then the field strength in the clump satisfies, $B_{clump} \sim 2\pi G^{1/2} \Sigma_{clump}$ for clump mass column density Σ_{clump} (Sect. 2). The magnetic force per unit volume acting on the clump by the field lines it drags behind is approximately $F_B = B_{clump}^2 / (8\pi R_{clump}) \sim G\Sigma_{clump}^2 / R_{clump}$. The force per unit volume acting on the clump by the gravity from the rest of the cloud is $F_G \sim G\Sigma_{cloud}\rho_{clump} \sim G\Sigma_{cloud}\Sigma_{clump}/R_{clump}$. Thus the ratio of the magnetic to the gravitational forces acting on the clump from the surrounding cloud is

$$F_B / F_G \sim \Sigma_{clump} / \Sigma_{cloud} >> 1. \tag{7}$$

This latter inequality is usually satisfied because protostellar clumps have low angular filling factors, which means their column densities are higher than the average cloud column densities around them. As a result, clumps do not free fall in a cloud until either their magnetic field lines become detached or their fields diffuse out. This is one of the reasons why clump motions can be slow.

Magnetic fields should also limit clump accretion from remote parts of the cloud. The magnetic force per unit volume exerted on the ambient gas in a cloud is $\sim B_{cloud}^2 / (8\pi R_{cloud}) \sim G\Sigma_{cloud}^2 / R_{cloud}$. The gravitational accretion force per unit volume that the clump exerts on this ambient gas is $\sim GM_{clump}\rho_{cloud}/R_{cloud}^2$. The magnetic to gravitational force ratio for accreted ambient cloud gas is

$$F_B / F_G \sim M_{cloud} / M_{clump} >> 1. \tag{8}$$

Thus the ambient cloud gas cannot freely fall onto a clump whose mass is significantly less than the mass of the whole cloud.

Pre-stellar clump motions and gas accretion onto clumps from remote parts of the cloud should be restrained by the cloud's magnetic field if it is close to the critical value. Pre-stellar clumps are therefore born with relatively slow speeds, and they should keep these speeds until their field lines detach. The protostars they form should accrete only from their immediate clump reservoirs or from closely interacting clumps. These protostars should also move slowly for a long time, even if they become detached from the field lines, because the protostars are bound to their clumps by clump gravity with a stronger acceleration ($G\Sigma_{clump}$) than

they are attracted to the whole cloud ($G\Sigma_{cloud}$), considering that $\Sigma_{clump} > \Sigma_{cloud}$. Protostars begin to move freely only when they become detached from the cloud's field lines and also destroy the clump that formed them. Before this detachment, protostars should appear offset from their clump centers with an equilibrium position that balances clump and cloud forces from magnetic fields, ram pressure, and gravity. The observation of slow protostellar and prestellar motions may eventually be used to determine the magnetic field strength. Faster motions compared to virial imply weaker fields compared to critical.

4. The Morphology of Destruction: Triggered Star Formation and Longevity in Molecular Cloud Envelopes

Jets, winds, heating, and ionization in dense cluster-forming cores can compress the existing clumps and produce tiny shells, both of which may trigger more star formation (Norman & Silk 1980; Quillen et al. 2005; Barsony 2007). If only low mass stars form, the energy input may not be disruptive and the core might survive for several crossing times. If high mass stars form, then the core should be rapidly dispersed. Gas exhaustion also halts star formation. In a region that forms a bound cluster, nearly half of the gas is converted into stars and little remains in a dense state for more star formation.

These two endings for core activity are readily observed. High mass cores that form O-type stars make compact HII regions in the midst of dense clusters of lower mass stars. These HII regions clear out small cavities at first and change the mode of star formation from one of collapse and turbulence compression to one of triggering at the cavity edges and in the debris. Low mass cores with no O-type stars should contain smaller, less energetic bubbles when they are young (Quillen et al. 2005) and a gradual lessening of extinction over time as the gas gets used up, rather than an explosive clearing. The efficiency may reach $\sim 30\%$ by the clearing time in both cases (Lada & Lada 2003). The age of a newly cleared cluster is typically short, only a few crossing times.

The general speed up of star formation with density implies that GMC cores are finished before the diffusion time in the envelope. This is particular true if the GMC envelope is subcritical, which seems likely (Sect. 2). In addition, GMCs in the main disk of the Milky Way have an average column density equivalent to ~ 10 mag of visible extinction (Solomon et al. 1987). Because it takes ~ 4 magnitudes for a clumpy cloud to significantly shield the background uv light (McKee 1989; Ciolek & Mouschovias 1995; Myers & Khersonsky 1995; Padoan et al. 2004), there should be considerable ionization in the envelopes of GMCs. This means the magnetic diffusion time can be long, many tens of dynamical times. Thus we have an exception to the highly dynamical picture presented in the preceding sections:

GMC envelopes can be relatively long-lived.

Envelope longevity appears necessary also from the Zuckerman & Evans (1974) constraint, which suggests that CO clouds cannot be collapsing as a whole, and from the Solomon, Sanders & Scoville (1979) constraint, which notes that the inner Galaxy is highly molecular (Sect 3.1). Dynamical evolution of GMCs means primarily that they progress toward star formation relatively quickly and then scatter their envelopes relatively quickly. But it does not mean that the scattered envelope disappears.

An example of rapid star formation with slow GMC envelope evolution is shown in Figure 5, which reproduces the southern part of the inner spiral arm in M51 from the HST Heritage mosaic. There is a clear progression of star formation morphology from left (east) to right that matches the expected time evolution as the gas flows away from the spiral shock. In the east, there is a large concentrated dark cloud that is part of the dust lane itself. It measures 1.0×0.23 kpc^2 (assuming the distance is 9.5 Mpc from Zimmer et al. 2004) and with an estimated average visual extinction of 2 mag, contains 10^7 M$_\odot$. Star formation occurs throughout this cloud in several places, so there is no perceptible time delay between cloud formation and star formation. The giant cloud itself is a "giant molecular association" or "supercloud," and the relatively small concentrations in it, barely visible at ~ 100 pc in length, would be the GMCs. This size and hierarchical morphology is common in the spiral arms of our Galaxy too (Grabelski et al. 1987). In the middle of the image there is relatively little in the center of the dust lane but there is one kpc-long clumpy cloud extending south and there are several small cloud filaments to the west of it, along with many small HII regions in the dense knots. The small filaments make irregular shells, and there are many bright blue stars inside these shells that could have pressurized them. Further to the west there is another supercloud with embedded HII regions inside the dustlane and there are two other kpc-scale filaments south of the dustlane and aligned perpendicular to it ("feathers" – Shetty & Ostriker 2006; La Vigne, Vogel & Ostriker 2006). These filaments have low-level star formation along their edges. There are also more blue stellar associations between the filaments, giving the overall appearance of shells again. By shells, we do not mean three-dimensional objects; the in-plane dimensions are much larger than the gas scale height, so these are more like ribbons or loops in the plane. The observed progression from left to right in the figure is the flow direction for gas in the density wave crest. Each feather has swung out counter-clockwise from the dust lane because of reverse shear on the inner side of the arm (Balbus 1988; Kim & Ostriker 2002, 2006). The time scale for this is several tens of Myr at a relative speed of ~ 50 km s^{-1} (according to Kim & Ostriker 2006, the spur patterns move at the rotation speed of the disk relative to the arm).

The figure shows many aspects of the present discussion: the rapid appearance of cores

and stars in giant clouds that form in the dust lane, the shredding of these clouds downstream, the appearance of 500-pc scale star complexes and their 80-pc knots, which are OB associations in the classic definition, the diffuse, filamentary and shell-like nature of the cloudy debris, and the lingering star formation in the cores of this debris. Most of the dense cloud cores contain some level of star formation inside or immediately adjacent to them, and much of the diffuse filamentary gas has little star formation. Essentially all of the dark clouds should be molecular. The classical notion that there is a delay between the spiral shock and star formation is not evident: star formation is immediate in the superclouds. The offset between the main dustlanes and the blue light that has long been interpreted as a time delay for star formation is in fact from cloud distruction following dustlane emergence and from triggered and lingering second-generation star formation in the shear-twisted debris.

The time scale for evolution of the filaments, which are apparently the scattered envelopes of superclouds and GMCs, can be assessed from this figure. The smallest filaments in the image are $\sim$ 20 pc wide. For one magnitude of extinction and a depth equal to their width, they would have an H density of ~ 30 cm^{-3}. The bigger filaments would have slightly lower average densities because their extinctions look about the same. These structures resemble local diffuse clouds although they are probably molecular in M51, which is molecule-rich. The dynamical time at this density is $\sim$ 15 My, which is a good fraction of the spiral arm flow time represented in the figure. Since most of the filaments contain star formation inside or adjacent to their cores, the onset of star formation in the debris appears to operate relatively quickly, on approximately the dynamical time. This would seem to be impossible if the clouds are diffuse. Magnetic diffusion should be slow in the low-density parts of this gas because they are highly exposed to ambient starlight, and if the debris came from the disruption of sub-critical GMC envelopes, it should be sub-critical in filamentary form too.

The morphology of clouds and HII regions in Figure 5 gives a clue to the continued activity on relatively short time scales. There seem to be two mechanisms for second generation star formation: direct triggering from HII regions and other pressures associated with the existing blue stars, and gravity-driven streaming of gas along the filaments to make dense cores (e.g., Nakamura, Hanawa, & Nakano 1993; Tomisaka 1995; Fiege & Pudritz 2000). The first of these short-circuits the long diffusion time by compressing the gas (Sect. 3.5. The second overcomes magnetic resistance directly by increasing the mass-to-flux ratio, presumably to the supercritical point. The cores are well separated and the mass-to-flux ratio increases by the ratio of filament length divided by filament width, which is a factor of ~ 10. Gas that is sub-critical by a factor of 10 in low-density filaments can become supercritical when it collects to a core, and then it can collapse even if the rest of the filament has a long diffusion time. Filament streaming takes a time $\sim (L/W)\,(G\rho)^{-1/2}$ for collection length L

on each side of the core, filament width W, and filament density ρ. This time is longer than $(G\rho)^{-1/2}$ alone, but the process is still dynamical and it requires minimal magnetic diffusion before star formation begins in the core.

The low-density sub-critical debris left behind in the filaments should continue to have a lifetime significantly longer than the dynamical time because it is sub-critical and highly exposed. It satisfies the Zuckerman & Evans constraint and the Solomon, Sanders & Scoville constraint. But these constraints have little bearing on star formation time scales when they are satisfied by diffuse GMC debris. The fate of this gas depends more on supernovae and the clouds' pending impact with the next spiral arm.

We conclude that most or all of the gas that is strongly self-gravitating evolves toward star formation on a dynamical time, whether it is forming a first generation of stars in a supercloud or subsequent generations in the debris. A high fraction of the volume of the ISM is in the form of diffuse gas, which may evolve in isolation more slowly than the internal dynamical time considering the likely subcritical fields and strong ionic attachment to these fields. However, this diffuse gas is forced to evolve in other ways by supernovae and stellar pressures in its vicinity. Sometimes these pressures trigger star formation, speeding up magnetic diffusion and collapse locally, and sometimes they move the gas into tenuous shells and filaments that eventual get ionized and disperse. The full image of M51 indicates that many of the diffuse extinction clouds make it all the way to the next arm, so they last a relatively long time if they are left alone.

In a recent paper, Mouschovias, Tassis, & Kunz (2006) reviewed the observations which historically suggested slow ambipolar diffusion time scales for GMC evolution. The present model agrees with their assessment that cloud envelopes are subcritical and slow to evolve, and that cloud cores are supercritical and collapsing. However, they believe the cores form slowly on the ambipolar diffusion time and we suggest they form quickly because they are close to critical from birth or they are compressed. They also referred to the separation between dustlanes and HII regions in spiral density waves as evidence for long time scales prior to star formation, but we have shown for M51 that there is no such delay. The difference between these two views lies entirely in the different initial conditions for core formation, not in the theory of ambipolar diffusion and collapse. We also differ in our consideration of cloud disruption and secondary star formation, which can be rapid because of high stellar pressures.

There is no single mode of star formation but several, starting with what might be called a primary mode that begins with large scale gravitational instabilities in spiral arm dustlanes and elsewhere in the ambient ISM, continuing with triggered star formation during the disruption of the cores and envelopes in these primary clouds, and lingering further still

with the dynamical collapse of filamentary debris and more pressurized triggering during envelope dispersal. We believe considerable evidence supports a picture where the onset of star formation in almost all clouds is at the dynamical rate, not the slower ambipolar diffusion rate. The evidence also suggests that the complete destruction of clouds can be considerably slower, giving the molecules long total lifetimes. Thus cloud evolution consists of a mixture of rapid and slow processes. These are nicely mapped out as a time sequence in the downstream flow from a strong spiral arm. In galaxies with weak or no stellar spirals, the same phases of cloud evolution should occur, but they will be mixed together in space as there is no global trigger for the first stage.

5. IMF Variations for the 3 Modes of Star Formation

The previous sections presented evidence that star formation has three distinct modes: (1) rapid collapse for small stellar groups and single stars in turbulence-compressed regions, which may mix into clusters or remain dispersed, (2) rapid collapse of supercritical cores that are born with near-critical field strengths as a result of larger-scale galactic processes, and (3) supercritical collapse of single stars and clusters following slow, diffusion-limited contraction in an initially subcritical cloud. The latter is the standard model but appears to take too long for the general case and to give the wrong proportion of pre-stellar and stellar cores. The disruption of star-forming clouds was shown to involve another type of star formation, which is a variant of the first mode: triggered star formation in cloud envelopes and in debris from previous generations of stars. Examples of these modes were given and the whole evolutionary scenario was illustrated using HST Heritage images of M51.

These modes differ in fundamental ways so it is natural to expect some differences in the properties of stars they produce. The IMF, for example, could differ between quiescent regions in mode (3) and large-scale collapsing regions in mode (2). Turbulent fragmentation in mode (1) would seem to give a different IMF also. Binary fractions, mass segregation, efficiencies and other properties of star formation might differ as well. Remarkably, simulations with extremely diverse conditions, ranging from pure collapse with no magnetic fields (Bonnell & Bate 2006) to highly constrained and localized with strong fields (Tilley & Pudritz 2005) all give about the same IMF slope at intermediate mass. Simulations have not yet sampled out to high mass. The turnover at low mass depends on the assumptions of the model, and although the models can be tuned to give the right result, the origin of the turnover is not understood yet (compare, for example, the different reasons for a turnover in Padoan & Nordlund 2002, Martel et al. 2006, and Jappsen et al. 2005 or Bonnell, Clarke & Bate 2006).

Padoan & Nordlund (2002) and Padoan et al. (2007) discuss how magnetic turbulent compression with Kolmogorov-type scaling laws between velocity and length can partition the gas into pieces that have the Salpeter mass function at intermediate mass. Di Fazio (1986) and Elmegreen (1993, 1997) suggested a slightly different scenario where the IMF slope comes not only from instantaneous mass partitioning but also from differential collapse rates, which steepen the slope for the time-integrated population. Bonnell, Larson, & Zinnecker (2007) present a case for collapse without magnetic restraints, where gas can move freely relative to the dense cores and protostellar masses grow by competition accretion. We discussed how critical magnetic fields should limit this scenario in Section 3.7.

Turbulent fragmentation theories would seem to apply best to the first star formation mode. Competitive accretion seems to apply best to the second mode, i.e. to supercritical, collapsing, cluster-forming cores or parts of cores, where the magnetic field is relatively weak, clump motions are relatively unconstrained, and collapse motions dominate broad-spectrum turbulence for the dynamics. If this is the case, then we can assess what the possible IMF differences might be.

Bonnell, Larson, & Zinnecker (2007) show that in freely collapsing models, stellar masses grow mostly by accretion, sometimes from far away, and that stellar interactions and subcluster ejection limits the accretion for what turn out to be the low mass stars (e.g. Bate & Bonnell 2005). Bonnell & Bate (2006) note that competitive accretion works well for the high mass stars. The high masses of the highest mass stars can even run away in this model, because the accretion rate increases with mass (e.g., Martel et al. 2006). Also in dense cluster-forming cores, pre-stellar clumps might coalesce to make more massive stars (Peretto, André, & Belloche 2006). Thus mode 2 would seem to be able to produce an excess of massive stars if the density gets high and the gas reservoir is large, as in a massive cluster. This would make the mode 2 part of the IMF somewhat shallow. The mode 1 part of the same cloud would presumably not have such coalescence and runaway properties: each star is forced to accrete from its immediate neighborhood because of magnetic stresses. Then the IMF might be slightly steeper. The composite IMF in a cluster that contains both a supercritical collapsing inner core and a turbulence-compressed outer core or envelope would have an IMF gradient and an intermediate average IMF. The outer IMF would be steeper than the inner IMF, and the average would depend on what fraction of the total mass was in the supercritical collapsing state. Such a variation would naturally account for mass segregation at stellar birth and for the slight trend toward shallower IMFs with increasing density and pressure (Elmegreen 2004).

The Padoan & Nordlund (2002) model assumes the clump mass that forms in a compressed layer is proportional to ρL^3 for compressed density ρ and layer thickness L. The un-

compressed values are ρ_0 and L_0. By mass and flux conservation, $\rho L = \rho_0 L_0$ and $B\rho = B_0\rho_0$, so the magnetic field dominates the layer pressure, giving $\rho v = \rho_0 v_0$ for velocity dispersions v and v_0. With space partitioned as $P(k)d\log k = k^3 d\log k$ and velocity correlated in the surrounding cloud as $v_0/v_c = (L_0/R)^\alpha$ for cloud radius R, they get a power law mass function $f(M)d\log M = P(k)d\log k$ for $M = \rho L^3 = \rho_0 L_0 L^2 \propto \rho_0 L_0^3 \left(v/v_c\right)^2 \left(R/L_0\right)^{2\alpha}$. If the initial scale for the compression, L_0, is identified with the inverse wavenumber of the turbulence, k^{-1}, then $M \propto k^{2\alpha-3}$. Combining this with $P(k)$, the result is $f(M) \propto M^{3/(2\alpha-3)} \propto M^{-1.33}$ for $\alpha = 0.37$, from the velocity power spectrum. The analogous result for filaments is slightly different. Assuming again that $M = \rho L^3$ for filament width L, we now have conservation laws $\rho L^2 = \rho_0 L_0^2$ and $BL^2 = B_0 L_0^2$, which still gives $\rho \propto B \propto v$ by pressure balance, but then the mass becomes $M = \rho_0 L_0^2 L = \rho_0 L_0^3 \left(v/v_c\right)^{1/2} \left(R/L_0\right)^{\alpha/2} \propto k^{\alpha/2-3}$. With the same space partitioning, $P(k) \propto k^3$, this gives an IMF for filaments of $f(M) \propto M^{9/(\alpha-6)} \sim M^{-1.60}$, which is slightly steeper than the Salpeter function.

If the compressed layers produce a number of star formation sites proportional to the area layer, namely $\left(L_0/L\right)^2$, and the cylinders produce a number of sites proportional to the length, L_0/L, then both of these IMFs becomes $f(M) \propto M^{-1}$. This can be seen by using $P(k) = k^3 \left(L_0/L\right)^2 d\log k$ for the layer and $k^3 \left(L_0/L\right) d\log k$ for the filament, i.e., counting not just compression space in the original cloud (the k^3 term) but also the number of sites per compressed region. In the first case, $k^3 \left(L_0/L\right)^2 = k^3 \left(v_c/v\right)^2 \left(R/L_0\right)^{2\alpha} \propto k^{3-2\alpha}$ and in the second case $k^3 \left(L_0/L\right) = k^3 \left(v_c/v\right)^{1/2} \left(R/L_0\right)^{\alpha/2} \propto k^{3-\alpha/2}$. Because $M \propto k^{2\alpha-3}$ and $k^{\alpha/2-3}$ in the layer and filament geometries, the IMFs are simply M^{-1}. This is the usual result for hierarchical structure.

If the turbulence-compressed layers and filaments fragment into star formation sites in this way, giving $f(M) \propto M^{-1}$ in both cases, then the instantaneous mass spectrum from turbulence fragmentation would be shallower than the observed IMF. Also in this case, we should observe linear strings of the youngest pre-stellar condensations and protostars along gaseous filaments with a number of condensations increasing with filament length. We should see two dimensional arrays of condensations and protostars inside compressed layers with the number of condensations increasing with the area of the layer. To get the Salpeter IMF or something steeper requires additional physics. Elmegreen (1993, 1997) suggested this was the mass dependence of the dynamical timescale for evolution of gas into protostars: in a hierarchically structured cloud, the smaller pieces, which have lower masses, tend to be denser on average, and to have shorter dynamical times. Thus an instantaneous mass function from turbulence steepens into the IMF as proportionally more low mass clumps and stars form by turbulence compression and other dynamical processes.

The IMF is likely to be much more complicated than either theory predicts, and possibly

the result of a combination of effects. Vázquez-Semadeni, Kim & Ballesteros-Paredes (2005) for example, found that the collapsing mass increases as the relative magnetic field strength increases. This implies that the IMF in sub-critical regions of clouds, such as GMC envelopes and diffuse regions, might be shallower than the IMF in critical or super-critical regions where the field strength is relatively low. Such a trend would counter the mass segregation gradient discussed above.

6. Summary

The previous sections considered many facets of star formation that all fall under one basic model consisting of three tenets: (1) clouds of various origins are hierarchically structured as a result of turbulence and self-gravity, (2) their densest parts evolve toward star formation at about the local dynamical rate, and (3) their low-density envelopes disperse as a result of this star formation and survive in pieces for several dynamical times, possibly forming stars in multiple generations.

Cloud formation in the first step includes compression and gravitational collapse in spiral shocks, swing-amplified spiral arms, expanding shells and other dynamical structures that form by turbulence and stellar pressures on a wide range of scales. The formation and initial evolution occurs on the dynamical time scale, and in absolute terms, this can be large, several tens of millions of years, or small, a million years or less, depending on the pre-cloud density. The low density parts of these clouds, which are most directly exposed to background starlight, are most strongly tied to the magnetic field and evolve more slowly in relative terms than the dense, optically-thick cores. Core evolution starts close and stays close to the magnetically critical state, and with relatively little delay, becomes magnetically supercritical. At this point star formation proceeds at a high rate, which is still close to the dynamical rate but now at a high density. Star formation appear to accelerate as the cloud density increases, but observers at each stage would see it operating at only a few times the current dynamical rate even though relatively old stars are present. Star formation disrupts the core relatively quickly, with no intermediate stage of dynamical equilibrium.

The envelope becomes disrupted too, following core star formation, but if there is a relatively large internal magnetic field and a relatively slow diffusion rate, then it can be pushed to the side, broken, and dispersed without collapsing into stars immediately. The envelope also has star formation during this whole process, and it can be supercritical in small regions where turbulence compression and external pressures accelerate the diffusion rate. Star formation finally stops when all of the residual gas is converted back into a low-density, weakly self-gravitating state by starlight heating, ionization, and evaporation.

Cloudy debris that is relatively isolated and in a low pressure environment, such as the Taurus clouds, can form stars by the standard model, one at a time by quasi-equilibrium magnetic diffusion up to densities of 10^{10} cm^{-3} or so, as many models of this process suggest. The evidence suggests that most star formation is not like this, however.

During the entire cycle of cloud evolution, a large fraction of the molecular mass and a large fraction of the time are spent without significant star formation, which is confined primarily to the dense, short-lived inner regions. These dense regions form star clusters, and they do this by forming protostars with relatively low velocities that begin their lives inside gas filaments and hierarchical subunits and mix over time inside the cloud core. The outer parts may never get time to mix before core disruption. Then they remain hierarchical up to scales of hundreds of parsecs until galactic shear tears them apart.

The IMF would seem to be different for the three modes of star formation discussed here: turbulence compression promotes scale-free hierarchical structure while supercritical collapse promotes fast relative motions and large-scale accretion. Considering IMF simulations currently available, the supercritical cluster cores could form proportionally more massive stars, thereby contributing to mass segregation and a slight flattening of the IMF in dense, supermassive clusters.

I am grateful to the referee, Mark Krumholz, for useful suggestions, and to Jonathan Tan and Yancy Shirley for comments on the manuscript.

REFERENCES

Aarseth, S.J., & Lecar, M. 1975, ARAA, 13, 1

Allen, L., Megeath, S. T., Gutermuth, R., Myers, P. C., Wolk, S., Adams, F. C., Muzerolle, J., Young, E., & Pipher, J. L. 2007, in Protostars and Planets VI, ed. B. Reipurth, D. Jewitt, & K. Keil, (Tucson, Univ of Arizona), 361

Alves, J., Lombardi, M., & Lada, C.J. 2007, A&A, 462, L17

Bacmann, A., André, P., Puget, J.-L., Abergel, A., Bontemps, S., & Ward-Thompson, D. 2000, A&A, 361, 555

Balbus, S. A. 1988, ApJ, 324, 60

Ballesteros-Paredes, J., Hartmann, L., Vzquez-Semadeni, E. 1999, ApJ, 527, 285

Ballesteros-Paredes, J., & Mac Low, M.-M. 2002, ApJ, 570, 734

Ballesteros-Paredes, J., & Hartmann, L. 2007, Rev. Mexican A&A, 43, 123

Barsony, M. 2007, in Triggered Star formation in a turbulent ISM, ed. B.G. Elmegreen & J. Palous, IAU Symposium 237, (Cambridge: Cambridge Univ. Press), in press

Bash, F.N., Green, E., & Peters, W.L., III. 1977, ApJ, 217, 464

Basu, S. 1997, ApJ, 485, 240

Basu, S., & Mouschovias, T.C. 1995, ApJ, 452, 386

Basu, S., & Ciolek, G.E. 2004, ApJ, 607, L39

Bate, M.R., & Bonnell, I.A. 2005, MNRAS, 356, 1201

Battinelli, P., Efremov, Y., & Magnier, E.A. 1996, A&A, 314, 51

Belloche, A., André, P., & Motte, F. 2001, in From Darkness to Light: Origin and Evolution of Young Stellar Clusters, ASP Conference Proceedings, Vol. 243. eds. T. Montmerle & P. André, (San Francisco: ASP), p.313

Bertoldi, F., & McKee, C.F. 1992, ApJ, 395, 140

Beuther, H., & Schilke, P. 2004, Science, 303, 1167

Boily, C.M., & Kroupa, P. 2003, MNRAS, 338, 673

Bonnell, I.A. & Bate, M.R. 2006, MNRAS, 370, 488

Bonnell, I.A., Clarke, C.J., & Bate, M.R. 2006, MNRAS, 368, 1296

Bonnell, I.A., Larson, R.B., & Zinnecker, H. 2007, in Protostars and Planets VI, ed. B. Reipurth, D. Jewitt, & K. Keil, (Tucson, Univ of Arizona), 149

Boulanger, F., Falgarone, E., Puget, J.L., & Helou, G. 1990, ApJ, 364, 136

Bourke, T.L., Myers, P.C., Robinson, G., & Hyland, A.R. 2001, ApJ, 554, 916

Brogan, C.L., & Troland, T.H. 2001, ApJ, 550, 799

Brooke, T.Y., et al. 2007, ApJ, 655, 364

Ciolek, G.E., & Mouschovias, T.C. 1995, ApJ, 454, 194

Ciolek, G.E., & Basu, S. 2001, ApJ, 547, 272

Cortes, P.C., Crutcher, R.M., & Watson, W.D. 2005, ApJ, 628, 780

Cortes, P.C. & Crutcher, R.M. 2006, ApJ, 639, 965

Crutcher, R.M. 1999, ApJ, 520, 706

Crutcher, R.M. 2007, in Triggered Star formation in a turbulent ISM, ed. B.G. Elmegreen & J. Palous, IAU Symposium 237, (Cambridge: Cambridge Univ. Press), in press

Curran, R.L., Chrysostomou, A., Collett, J.L., Jenness, T., & Aitken, D.K. 2004, A&A, 421, 195

Dahm, S.E., & Simon, T. 2005, AJ, 129, 829

Dickey, J.M., McClure-Griffiths, N.M., Stanimirovic, S., Gaensler, B.M, & Green, A.J, 2001, ApJ, 561, 264

de Avillez, M.A., & Breitschwerdt, D. 2005, A&A, 436, 585

Di Francesco, J., André, P., & Myers, P.C. 2004, ApJ, 617, 425

Di Fazio, A. 1986, A&A, 159, 49

Draine, B.T., & Sutin, B. 1987, ApJ, 320, 803

Efremov, Y.N. 1978, Sov.Astron.Lett., 4, 66

Efremov, Y.N. 1995, AJ, 110, 2757

Efremov, Y.N., & Elmegreen, B.G. 1998, MNRAS, 299, 588

Elmegreen, B.G. 1979, ApJ, 232, 729 (E79)

Elmegreen, 1989, ApJ, 338, 178

Elmegreen, 1993, ApJ, 411, 170

Elmegreen, B.G. 1997, ApJ, 486, 944

Elmegreen, B.G. 2000, ApJ, 530, 277

Elmegreen, B.G. 2004, MNRAS, 354, 367

Elmegreen, B.G. 2005, in The many scales in the Universe, eds. J. C. del Toro Iniesta, et al. (Dordrecht: Kluwer). p. 99

Elmegreen, B.G., & Elmegreen, D.M. 1983, MNRAS, 203, 31

Elmegreen, B.G., & Clemens, C. 1985, ApJ, 294, 523

Elmegreen, B.G., & Elmegreen, D.M. 1987, ApJ, 320, 182

Elmegreen, B.G., Elmegreen, D.M., Leitner, S. 2003, ApJ, 590, 271

Fatuzzo, M., Adams, F.C. 2002, ApJ, 570, 210

Fatuzzo, M., Adams, F.C., & Myers, P.C. 2004, ApJ, 615, 813

Fiege, J.D., & Pudritz, R.E. 2000, MNRAS, 311, 105

Flower, D.R., Pinneau des Forêts, G., & Walmsley, C.M. 2005, A&A, 436, 933

Fukui, Y. 2007, in Triggered Star Formation in a Turbulent Interstellar Medium, ed. B. G. Elmegreen & J. Palouš, (Cambridge: Cambridge Univ Press), 40

Furuya, R.S., Kitamura, Y., & Shinnaga, H. 2006, ApJ, 653, 1369

Gammie, C.F., Lin, Y.-T., Stone, J.M., & Ostriker, E.C. 2003, ApJ, 592, 203

Gao, Y. & Solomon, P.M. 2004a, ApJ, 609, 271

Gao, Y., & Solomon, P.M. 2004b, ApJS, 152, 63

Glenn, J., Walker, C.K., & Young, E.T. 1999, ApJ, 511, 812

Glover, S.C.O., & Mac Low, M.-M. 2007, ApJ, 659, 1317

Goldreich, P., & Lynden-Bell, D. 1965, MNRAS, 130, 125

Gomez, M., Hartmann, L., Kenyon, S. J. & Hewett, R. 1993, AJ, 105, 1927

Grabelsky, D. A., Cohen, R. S., Bronfman, L., Thaddeus, P., & May, J. 1987, ApJ, 315, 122

Greaves, J.S., Holland, W.S., & Murray, A.G. 1995, ApJ, 297, L49

Gutermuth, R.A., Megeath, S.T., Pipher, J.L., Williams, J.P., Allen, L.E., Myers, P.C., & Raines, S. N. 2005, ApJ, 632, 397

Hartmann, L., Ballesteros-Paredes, J., & Bergin, E.A. 2001, ApJ, 562, 852

Heitsch, F., Slyz, A. D., Devriendt, J.E.G., Hartmann, L.W., & Burkert, A. 2006, ApJ, 648, 1052

Heydari-Malayeri, M., Charmandaris, V., Deharveng, L., Rosa, M. R., Schaerer, D., & Zinnecker, H. 2001, A&A, 372, 527

Heitsch, F., Zweibel, E., Slyz, A.D., & Devriendt, J.E.G. 2004, ApJ, 603, 165

Heitsch, F., Slyz, A.D., Devriendt, J.E.G., & Burkert, A. 2006, MNRAS, 373, 1379

Holland, W.S., Greaves, J.S., Ward-Thompson, D., & André, P. 1996, A&A, 309, 267

Honma, M., Sofue, Y., & Arimoto, N. 1995, A&A, 304, 1

Huff, E.M., & Stahler, S.W. 2006, ApJ, 644, 355

Hujeirat, A., Camenzind, M., & Yorke, H. W. 2000, A&A, 354, 1041

Iglesias-Páramo, J. et al. 2006, ApJS, 164, 38

Jappsen, A.-K., Klessen, R. S., Larson, R. B., Li, Y., & Mac Low, M.-M. 2005, ApJ, 435, 611

Jijina, J., Myers, P.C., & Adams, F.C. 1999, ApJS, 125, 161

Johnstone, D., Fich, M., Mitchell, G. F., & Moriarty-Schieven, G. 2001, ApJ, 559, 307

Johnstone, D., Wilson, C. D., & Moriarty-Schieven, G., et al. 2000, ApJ, 545, 327

Jørgensen, J.K., Johnstone, D., Kirk, H., & Myers, P.C. 2007, ApJ, 656, 293

Kamaya, H., & Nishi, R. 2000, ApJ, 543, 257

Kawamura, A., Minamidani, T., Mizuno, Y., Onishi, T., Mizuno, N., Mizuno, A., Fukui, T. 2007, in Triggered Star Formation in a Turbulent Interstellar Medium, ed. B. G. Elmegreen & J. Palouš, (Cambridge: Cambridge Univ Press), 101

Kennicutt, R.C., Jr. 1998, ApJ, 498, 541

Kim, W.-T. 2007, in Triggered Star formation in a turbulent ISM, ed. B.G. Elmegreen & J. Palous, IAU Symposium 237, (Cambridge: Cambridge Univ. Press), in press

Kim, W.-T., Ostriker, E.C., & Stone, J.M. 2002, ApJ, 581, 1080

Kim, W.-T., & Ostriker, E. C. 2002, ApJ, 570, 132

Kim, W.-T., & Ostriker, E. C. 2006, ApJ, 646, 213

Kim, W.-T., & Ostriker, E. C. 2007, ApJ, 660, 1232

Kirk, J.M., Ward-Thompson, D., & André, P. 2005, MNRAS, 360, 1506

Kirk, J.M., Ward-Thompson, D., & André, P. 2007, MNRAS, 375, 843

Koda, J., Sawada, T., Hasegawa, T., Scoville, N.Z. 2006, ApJ, 638, 191

Kroupa, P. 2001, MNRAS, 322, 231

Krumholz, M.R., & McKee, C.F. 2005, ApJ, 630, 250

Krumholz, M.R., Matzner, C.D., & McKee, C.F. 2006, ApJ, 653, 361

Krumholz, M.R., & Tan, J.C. 2007, ApJ, 654, 304

Kudoh, T.., & Basu, S. 2007, in Triggered star formation in a turbulent interstellar medium, IAU Symposium 237, eds. B.G. Elmegreen & J. Paloš, (Cambridge: Cambridge Univ Press), in press

Lada C. J., Margulis M., & Dearborn D., 1984, ApJ, 285, 141

Lada, C.J., & Lada, E.A. 2003, ARAA, 41, 57

Lai, S.-P., Crutcher, R.M., Girart, J.M., & Rao, R. 2002, ApJ, 566, 924

Larson, R.B. 1981, MNRAS, 194, 809

La Vigne, M.A., Vogel, S.N., & Ostriker, E.C. 2006, ApJ, 650, 818

Lee, C.W., & Myers, P.C. 1999, ApJS, 123, 233

Lee, C.W., Myers, P.C., & Tafalla, M. 2001, ApJS, 136, 703

Leisawitz, D., Bash, F.N., & Thaddeus, P. 1989, ApJS, 70, 731

Li, P.S., Norman, M.L., Mac Low, M.-M., & Heitsch, F. 2004, ApJ, 605, 800

Li, Z.Y., & Nakamura, F. 2002, ApJ, 578, 256

Li, Z.Y., & Nakamura, F. 2004, ApJ, 609, L83

Li, Z.-Y. & Nakamura, F. 2006, ApJ, 640, L187

Lintott, C.J. et al. 2005, ApJ, 620, 795

Mac Low, M.-M. 1999, ApJ, 524, 169

Mac Low, M.-M., Klessen, R. S., Burkert, A., & Smith, M. D. 1998, Phys. Rev. Lett., 80, 2754

Mac Low, M.-M., & Klessen, R.S. 2004, RvMP, 76, 125

Martel, H., Evans, N.J., II., & Shapiro, P.R. 2006, ApJS, 163, 122

Matthews, B.C., Lai, S.-P., Crutcher, R.M., & Wilson, C.D. 2005, ApJ, 626, 959

McKee, C.F. 1989, ApJ, 345, 782

McKee, C. F., Zweibel, E. G., Goodman, A. A., & Heiles, C. 1993, in Protostars and Planets III, ed. E.H. Levy & J.I. Lunine, (Tucson: Univ. Arizona Press), 327

Mestel, L. 1965, QJRAS, 6, 265

Motte, F., André, P., & Neri, R. 1998, A&A, 336, 150

Motte, F., André, P., Ward-Thompson, D., & Bontemps, S. 2001, A&A, 372, L41

Mouschovias, T.C. 1976, ApJ, 207, 141

Mouschovias, T.C. 1991, in The Physics of Star Formation and Early Stellar Evolution, ed. C.J. Lada & N. D. Kylafis (Dordrecht: Klewer), 449

Mouschovias, T.C., & Spitzer, L., Jr. 1976, ApJ, 210, 326

Mouschovias, T.C., Tassis, K., & Kunz, M.W. 2006, ApJ, 646, 1043

Myers, P.C. 2005, ApJ, 623, 280

Myers, P.C., Fuller, G.A., Goodman, A.A., & Benson, P.J. 1991, ApJ, 376, 561

Myers, P.C., & Khersonsky, V.K. 1995, ApJ, 442, 186

Nakamura, F., & Li, Z.-Y. 2005, ApJ, 631, 411

Nakamura, F. & Li, Z.-Y. 2007, ApJ, 662, 395

Nakamura, F., Hanawa, T., & Nakano, T. 1993, PASJ, 45, 551

Nakano, T. 1998, ApJ, 494, 587

Nakano, T. & Tademaru, E. 1972, ApJ, 173, 87

Nakano, T., & Nakamura, T. 1978, PASJ, 30, 671

Nakano, T., & Umebayashi, T. 1986, MNRAS, 218, 663

Nanda Kumar, M. S., Kamath, U. S., Davis, C. J. 2004, MNRAS, 353, 1025

Norman, C. & Silk, J. 1980, ApJ, 238, 158

Omont, A. 1986, A&A, 164, 159

Onishi, T., Mizuno, A., Kawamura, A., Tachihara, K., & Fukui, Y. 2002, ApJ, 575, 950

Padoan, P., Juvela, M., Bally, J., & Nordlund, A. 1998, ApJ, 504, 300

Padoan, P., & Nordlund, A. 1999, ApJ, 526, 279

Padoan, P., & Nordlund, A. 2002, ApJ, 576, 870

Padoan, P., Willacy, K., Langer, W., & Juvela, M. 2004, ApJ, 614, 203

Padoan, P. & Scalo, J. 2005, ApJ, 624, L97

Padoan, P., Nordlund, A., Kritsuk, A.G., Norman, M.L. 2007, astroph/0701795

Palla, F., & Stahler, S.W. 2000, ApJ, 540, 255

Pan, K., Federman, S.R., Sheffer, Y., & Anderson, B.-G. 2005, ApJ, 633, 986

Patel, K., & Pudritz, R.E. 1994, ApJ, 424, 488

Pelupessy, F.I., Papadopoulos, P.P., & van der Werf, P. 2006, ApJ, 645, 1024

Peretto, N., André, Ph., & Belloche, A. 2006, A&A, 445, 979

Pinto, F. 1987, PASP, 99, 1161

Piontek, R.A., & Ostriker, E.C. 2005, ApJ, 629, 849

Polk, K. S., Knapp, G. R., Stark, A. A., & Wilson, R. W. 1988, ApJ, 332, 432

Quillen, A., Thorndike, S., Cunningham, A., Frank, A., Gutermuth, R., Blackman, E., Pipher, J., & Ridge, N. 2005, ApJ, 632, 941

Rand, R.J., & Kulkarni, S.R. 1990, ApJ, 349, L43

Roberts, D.A., Crutcher, R.M., & Troland, T.H. 1997, ApJ, 479, 318

Rosolowsky, E. & Blitz, L. 2005, ApJ, 623, 826

Ryden, B.S. 1996, ApJ, 471, 822

Scoville, N.Z., & Solomon, P.M. 1975, ApJ, 199, L105

Shetty, R., & Ostriker, E.C. 2006, 647, 997

Shu, F.H. 1983, ApJ, 273, 202

Shu, F.H., Adams, F.C., & Lizano, S. 1987, ARAA, 25, 23

Smith, M.D., Gredel, R., Khanzadyan, et al. 2005, MmSAI, 76, 247

Solomon, P. M., Sanders, D. B., & Scoville, N. Z. 1979, in The large-scale characteristics of the galaxy, ed. W.B. Burton, (Dordrecht: Reidel) p. 35

Solomon, P. M., Rivolo, A. R., Barrett, J., & Yahil, A. 1987, ApJ, 319, 730

Stanke, T., Smith, M.D., Gredel, R., & Khanzadyan, T. 2006, A&A, 447, 609

Steinacker, J., Bacmann, A., Henning, Th., Klessen, R., & Stickel, M. 2005, A&A, 434, 167

Stone, J. M., Ostriker, E. C., & Gammie, C. F. 1998, ApJ, 508, L99

Stützki, J., Bensch, F., Heithausen, A., Ossenkopf, V., & Zielinsky, M. 1998, A&A, 336, 697

Tachihara, K., Onishi, T., Mizuno, A., & Fukui, Y. 2002, A&A, 385, 909

Tafalla, M., Mardones, D., Myers, P.C., Caselli, P. Bachiller, R., & Benson, P.J. 1998, ApJ, 504, 900

Tan, J.C., Krumholz, M.R., & McKee, C.F. 2006, ApJ, 641, L121

Tassis, K., & Mouschovias, T.C. 2004, ApJ, 616, 283

Testi, L., Sargent, A.I., Olmi, L et al. 2000, ApJ, 540, 53

Testi, L., & Sargent, A. I. 1998, ApJ, 508, L91

Tilley, D.A. & Pudritz, R.E. 2005, JRASC, 99, 132

Tomisaka, K. 1995, ApJ, 438, 226

Tomisaka, K., Ikeuchi, S., & Nakamura, T. 1988, ApJ, 335, 239

Tomisaka, K., Ikeuchi, S., & Nakamura, T. 1990, ApJ, 362, 202

Troland, T.H., Crutcher, R.M., Goodman, A.A., Heiles, C., Kazès, I., & Myers, P.C. 1996, ApJ, 471, 302

Uchida, K.I., Fiebig, D., & Güsten, R. 2001, A&A, 371, 274

Umebayashi, T., & Nakano, T. 1990, MNRAS, 243, 103

Vacca, W.D., Garmany, C.D., & Shull, J.M. 1996, ApJ, 460, 914

Vázquez-Semadeni, E., Kim, J., & Ballesteros-Parades, J. 2005, ApJ, 630, L49

Vázquez-Semadeni, E., Kim, J., Shadmehri, M., & Ballesteros-Paredes, J. 2005, ApJ, 618, 344

Verschueren, W. 1990, A&A, 234, 156

Verschuur, G.L. 1993, AJ, 106, 2580

Walsh, A.J., Myers, P.C., & Burton, M.G. 2004, ApJ, 614, 194

Walsh, A.J., Bourke, T.L., & Myers, P.C. 2006, ApJ, 637, 860

Walsh, A.J., Myers, P.C., Di Francesco, J., Mohanty, S. Bourke, T.L., Gutermuth, R., & Wilner, D. 2007, ApJ, 655, 958

Whitworth, A. 1979, MNRAS, 186, 59

Williamsn, J.P. & McKee, C.F. 1997, ApJ, 476, 166

Williams, J.P., Myers, P.C., Wilner, D.J., & Di Francesco, J. 1999, ApJ, 513, L61

Williams, J.P., & Myers, P.C. 1999, ApJ, 518, L37

Williams, J.P., Lee, C.W., & Myers, P.C. 2006, ApJ, 636, 952

Wong, T. & Blitz, L. 2002, ApJ, 569, 157

Wu, J., Evans, N.J., II., Gao, Y., Solomon, P.M., Shirley, Y.L., & Vanden Bout, P.A. 2005, ApJ, 635, L173

Wu, Y., Zhu, M., Wei, Y., Xu, D., Zhang, Q., Fiege, J.D. 2005, ApJ, 628, L57

Zimmer, P., Rand, R. J., & McGraw, J. T. 2004, ApJ, 607, 285

Zuckerman, B., & Evans, N.J. II 1974, ApJ, 192, L149

Zweibel, E.G. 2002, ApJ, 567, 962

This preprint was prepared with the AAS LaTeX macros v5.2.

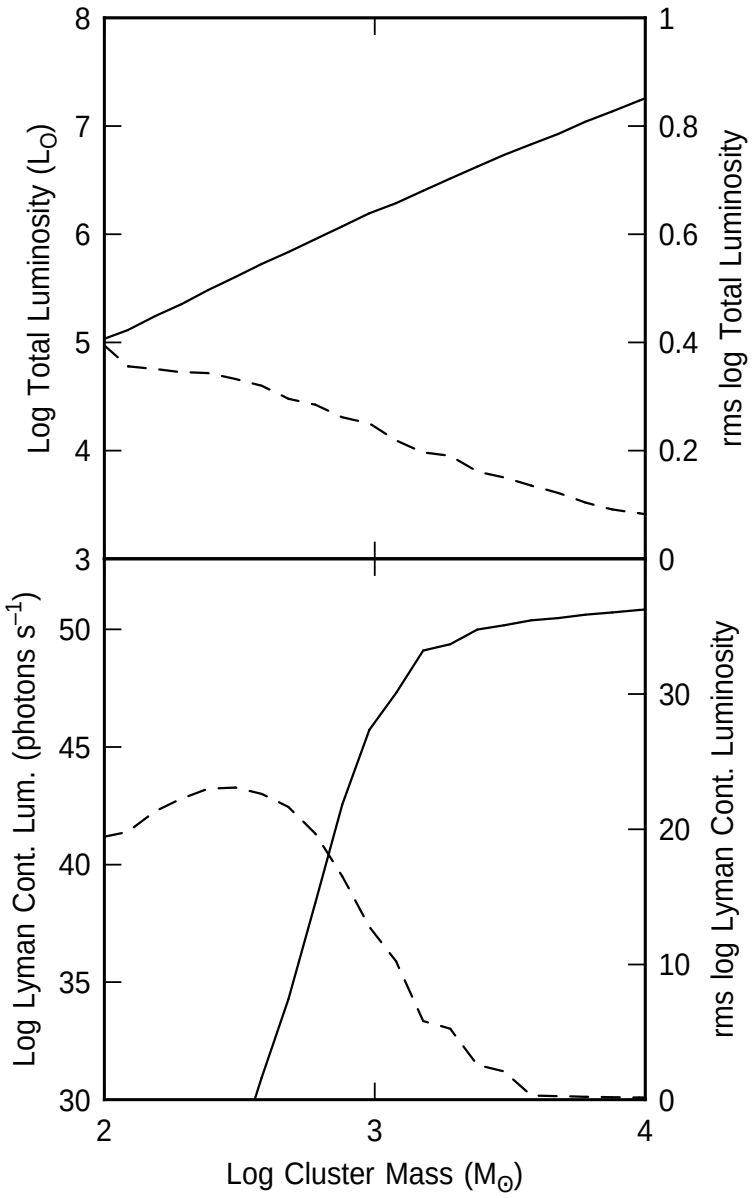

Fig. 1.— (bottom) The Lyman continuum luminosity in photons per second (solid line) is shown versus the cluster mass, using data in Vacca et al. (1996). 1000 cluster samples are made for each mass, and each cluster is formed by randomly sampling an IMF. The dashed line (right-hand axis) shows the rms deviation around the average luminosity that comes from the stochastic sampling. The Lyman continuum luminosity sharply increases for clusters more massive than $\sim 10^3$ $M_\odot$ because this is the mass where the IMF is typically sampled out to the O-star range. (top) The total luminosity of the cluster is shown versus the cluster mass, along with the rms deviations from the sampling.

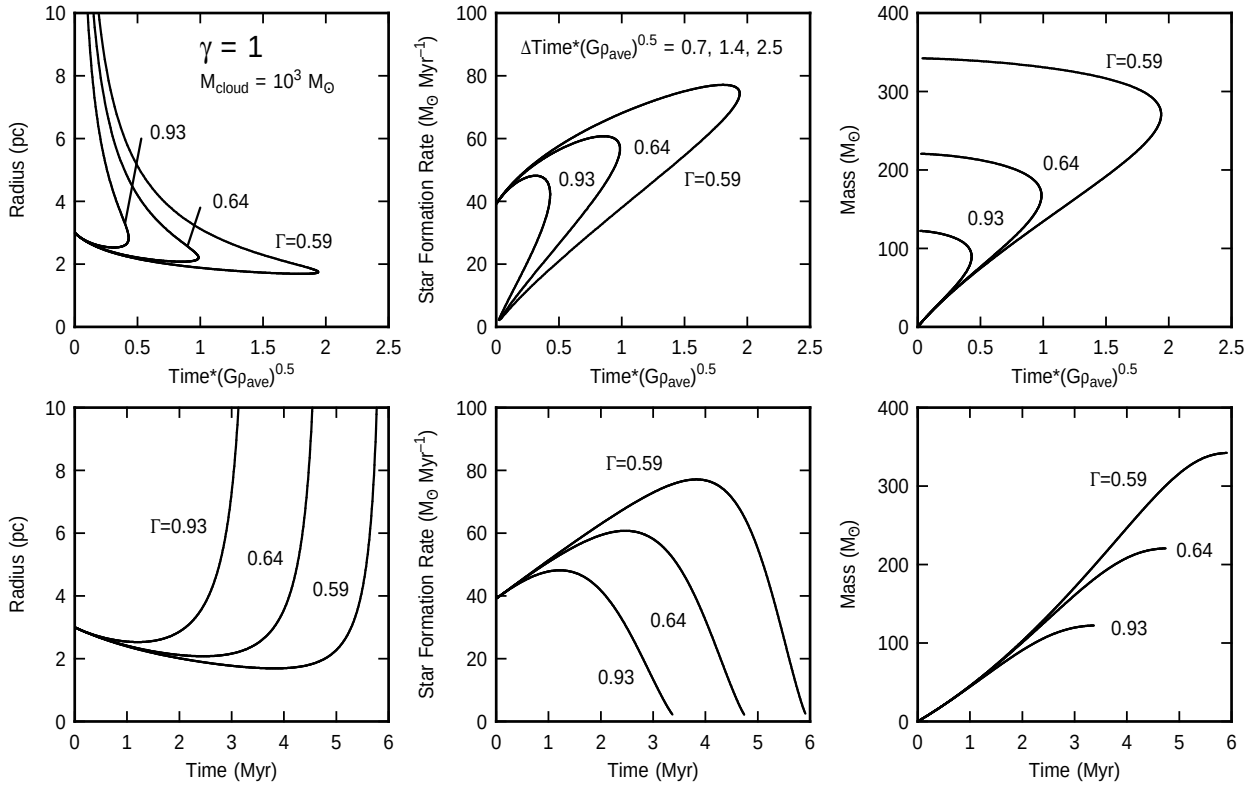

Fig. 2.— Models based on the Huff & Stahler (2006) formulism with energy input from stars. The bottom panels show cloud radius, star formation rate, and cluster mass versus the absolute time, and the top panels show these quantities versus the relative time, which is the absolute time divided by the instantaneous dynamical time for the average density inside the cloud. The numbers in the top middle panel are the product of the instantaneous crossing rate at the peak in the star formation rate (and at the peak density) multiplied by the duration of star formation, which is the time interval between the half-peaks in the star formation rate shown in the lower middle panel. These models assume the luminosity of the cluster increases linearly with cluster mass ($\gamma = 1$) and they assume the initial cloud mass is 10^3 $M_\odot$. This would be analogous to the Taurus clouds or other regions of low-mass star formation. The total duration of star formation can be long in absolute terms, so fairly old stars can be present in such a region (as indicated by the long absolute times in the lower panels), but the main activity is always finished in only a few instantaneous crossing times, as indicated by the small values of $\Delta\mathrm{Time}\,(G\rho)^{0.5}$ in the top middle panel.

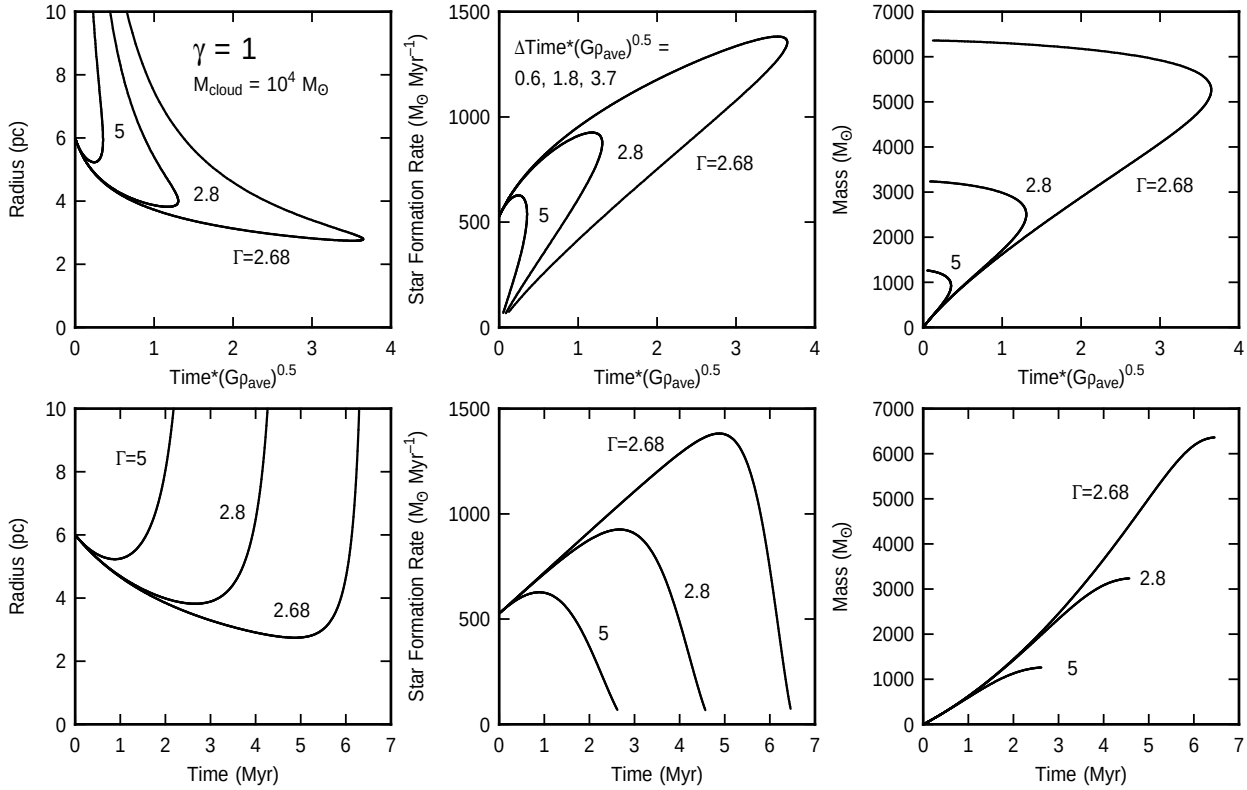

Fig. 3.— The same cluster formation model as in Fig. 2 except for a cloud mass of 10^4 $M_\odot$. The collapse of massive clouds is difficult to turn around by non-ionizing radiation, which is the case for this $\gamma = 1$ run. This is unrealistic, however, because such a massive cloud will form high-mass stars and then $\gamma >> 1$. $\Gamma = 2.68$ is an extreme case because it forms too many stars (a 64% final efficiency).

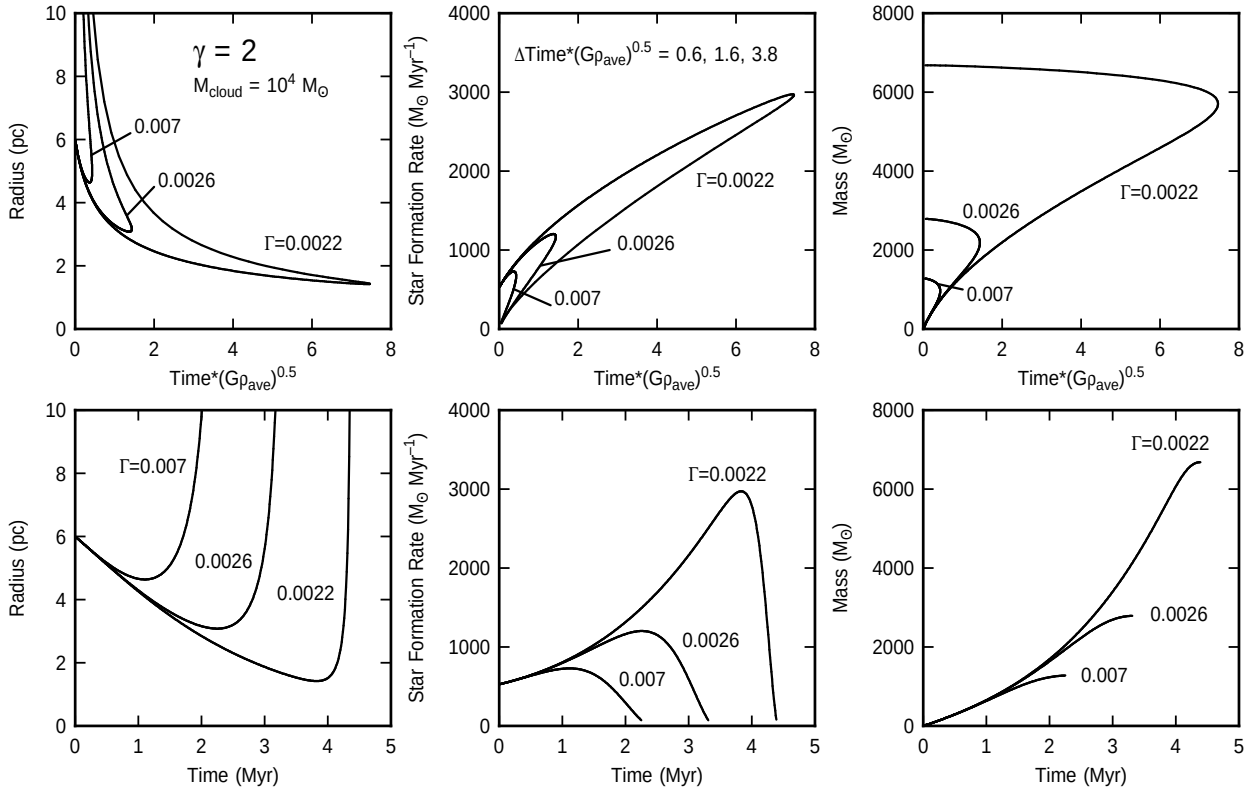

Fig. 4.— The cluster formation model with the same high mass as in Fig. 3, except now with a sensitive relation between cluster mass and luminosity using $\gamma = 2$. This model applies to high mass regions that form O-type stars. As in the other models, the duration of star formation is always short in terms of the instantaneous crossing time, but the total age span for the stars can be large in absolute terms. $\Gamma = 0.0022$ is an extreme case because it forms too many stars (a 67% final efficiency).

Fig. 5.— A section of the southern inner arm of M51 from the full-resolution Hubble Heritage image. The overall dimensions are 3.49 by 1.65 kpc. There are 2 giant cloud complexes in the main dust lane (10^7 $M_\odot$). Each has embedded HII regions, showing that star formation begins very soon after cloud formation with no significant downstream displacement. The post-shock flow is mostly from left to right in this figure as the gas streams along the spiral arm. The feathers of dust clouds below the main dust lane are twisted remnants of former cloud complexes in which star formation has dispersed the cores. Many filaments or ribbons of dust surround complexes of bright blue stars, suggesting pressurized dispersal. Star formation lingers in the filaments and in other debris because of triggering from these pressures and because of parallel collapse along the filaments into dense knots. The lowest density regions do not show star formation. These low density regions are presumably the envelopes and shredded debris of former GMCs. They appear to last a relatively long time; some even get to the next spiral arm (not shown) [Image degraded for astroph].